Digital processing of back-scatter electron imagery: A microscopic approach to quantifying chemical weathering

Ronald I. Dorn *Geography Department, Arizona State University, Tempe, Arizona 85287-0104*

ABSTRACT

This paper introduces digital processing of back-scattered electron (BSE) imagery as a microscopic approach to measure porosity from in situ dissolution of minerals. Four case studies exemplify this technique. Cases 1 and 2 explore the initiation and maintenance of weathering forms. In case 1, alveoli start in the Sedona area of Arizona when sandstone porosity exceeds ~32%. This threshold is probably the point at which intergrain cohesion is reduced enough for shear stresses to erode grains. Case 2 examines the maintenance of gnamma pits and polygonal cracks on a basalt boulder on the island of Maui, Hawaii. Rock dissolution progresses while the surface of the rock is preserved under coatings of silica glaze. When a porosity of ~37%–47% is reached, the weathering rind loses cohesion and spalls. Then, the protective silica glaze starts to accrete again, and another cycle begins.

Cases 3 and 4 involve measuring rates of dissolution over thousands of years. Case 3 concerns rock dissolution in weathering rinds formed on ventifacted aplite boulders. Weathering rinds lost mass for the last 14 k.y. at a rate of 40 ± 15 g/m^2/k.y., and for the last 17 k.y. at a rate of 43 ± 16 g/m^2/k.y. Dissolution rates increased over time to 67 ± 23 g/m^2/k.y. for the last 60–65 k.y. Case 4 addresses the classic topic of which variable is most important in chemical weathering: temperature, precipitation, or microenvironment. In situ measurements of plagioclase dissolution in ~3-k.y.-old basalt flows reveal that warmer temperatures enhance rates of plagioclase dissolution by about 0.07%/°C, when precipitation and microenvironment are controlled. Plagioclase dissolution increases as precipitation increases at higher elevations, even though temperature decreases. However, microenvironment is a more important control on plagioclase dissolution; organic-rich positions (under lichens) weather two to seven times faster than adjacent organic-poor positions away from epilithic organisms and rock coatings.

Rates of rock weathering are often established indirectly, by measuring the erosion of weathered material. In contrast, this microscopic method measures only in situ weathering. Conventional measures of rock weathering usually involve units, for example, depth of weathering pits or thickness of weathering rinds, that are not readily comparable to other data. In contrast, cases 3 and 4 illustrate that in situ measurements of rock and mineral porosity can yield data on mass weathered per unit area over time. This information is comparable to mass balance approaches in watershed- and soil-based weathering research.

INTRODUCTION

Weathering is the in situ breakdown and decay of minerals and rocks by biochemical and physical processes (Yatsu, 1988; Nahon, 1991). Weathering is a key research and pedagogic topic in the earth sciences, because it is the interface at which the crust interacts with the atmosphere, biosphere, and hydrosphere. Spatial variations in weathering processes influence the character of soil, fluvial, mass wasting, eolian, glacial, and coastal processes and landforms (e.g., Twidale, 1982; Brimhall and Dietrich, 1987; Brimhall et al., 1988; Lundqvist, 1988; Caine, 1992; Colin et al., 1992; Young and Young, 1992; McLennan, 1993).

Although physical, biological, and chemical weathering are synergistic and difficult to separate (Brimhall et al., 1991; Colin et al., 1992; Pope et al., 1995), this paper focuses on chemical weathering. Chemical weathering is increasingly being recognized as an important player in the earth system. Ca- and Mg-silicate weathering influences long-term climate through the capture of CO_2 (Brady, 1991; Velbel, 1993a; Probst et al., 1994; Gibbs and Kump, 1994). Chemical weathering is similarly important in evolutionary biology (Schwartzman and Volk, 1991), rock permeability (Fuller and Sharp, 1992), stone conservation (Emery, 1960; Paradise, 1993), acid rain studies (Meierding, 1993a), geochronology (Birkeland, 1984), paleoenvironmental research (Danin, 1985; Alpers and Brimhall, 1988; Yapp and Poths, 1992; Clemens et al., 1993; Bird et al., 1993), geoarchaeology (Lyman and Fox, 1989; Benito et al., 1993), glaciology (Souchez et al., 1990), soils (Dixon et al., 1984; Brimhall et al., 1991; Merritts et al., 1992; Colin et al., 1992), planetary geology (Gibson et al., 1982), ore deposits (Alpers and Brimhall, 1989; Colin et al., 1993b), fossil fuels exploration (Giles and Marshall 1986), and environmental biogeochemistry (Likens et al., 1977).

The purpose of this paper is to introduce and exemplify a microscopic approach to the quantification of chemical weathering that can be used as a stand-alone tool, or integrated with other techniques. Digital image processing of back-scattered electron (BSE) microscope imagery is presented here as a means of measuring pores from the in situ dissolution of minerals. Pores appear dark in a BSE image, which contrasts greatly with the surrounding mineral material that appears bright (Fig. 1). Image processing quantifies porosity by automated procedures that count the dark pore space. Digital image processing (Jensen, 1986) and BSE (Krinsley and Manley, 1989; Braun et al., 1990; Colin et al., 1992) have been combined previously to quantify porosity in petroleum research (Ehrlich et al., 1991), but not to quantify chemical weathering.

Data Repository item 9519 contains additional material related to this article.

GSA Bulletin; June 1995; v. 107; no. 6; p. 725–741; 14 figures; 1 table.

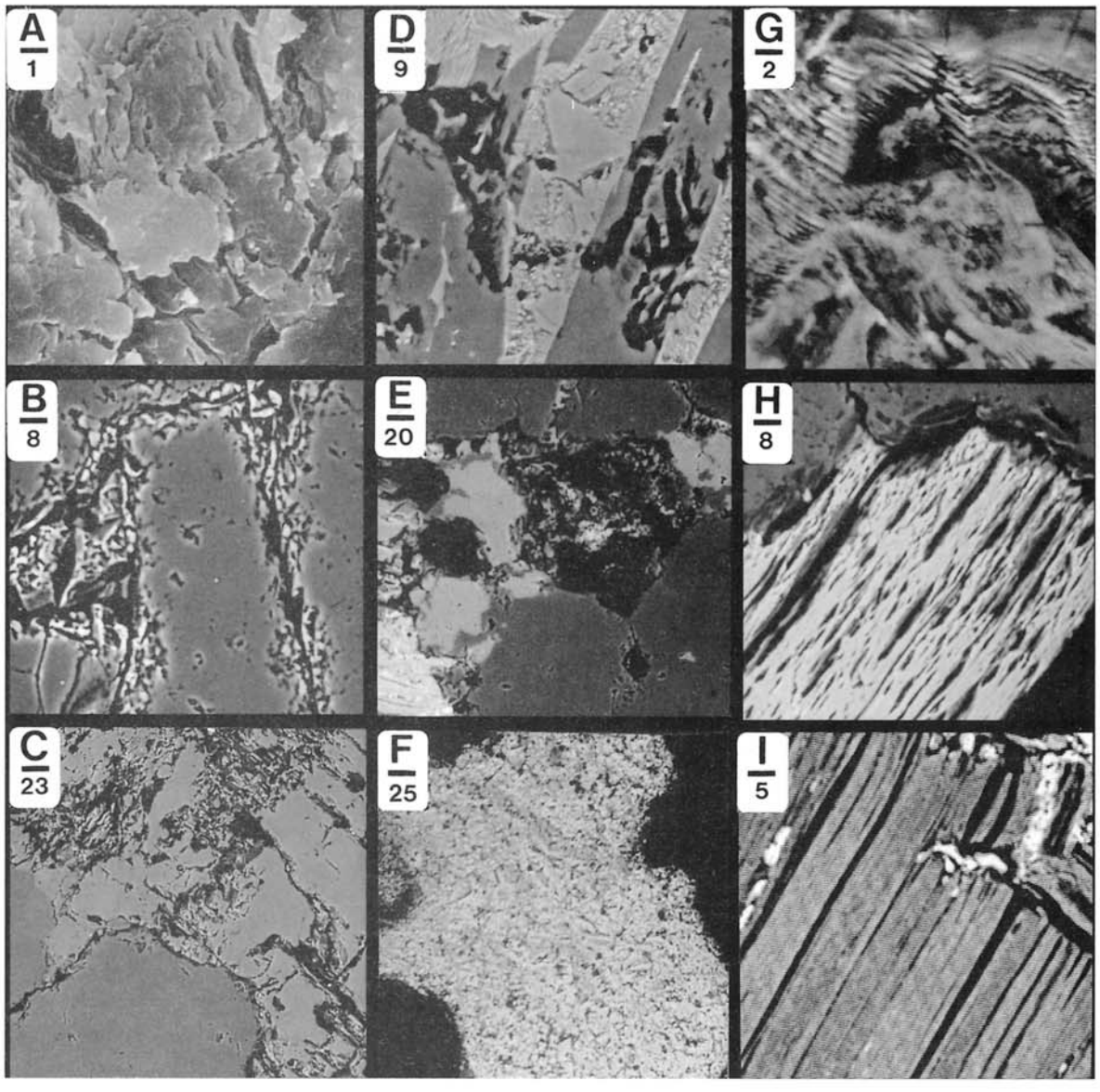

Figure 1. BSE (except 1A) images of different weathered minerals. Scale bars in micrometers. (A) Secondary electron micrograph of clay minerals in a weathering rind on a ventifacted boulder from Bishop Creek, eastern California. The clay minerals (with a clear Al signal in energy dispersive analyses) in the center cannot be readily distinguished from the weathered quartz on the right and lower left corners. (B) Dissolution of quartz, from regolith at Cabo San Lucas, Baja California. The polished section was placed in a barium chloride solution, and the Ba was sorbed by the weathering front—giving those locales of active weathering a brighter appearance, due to the high Z of Ba. (C) Dissolution of the brighter orthoclase (upper right) is greater than the darker quartz (lower left), from same site as 1A. (D) Dissolution of the darker plagioclase is greater than the surrounding olivine and clinopyroxene, from the weathering rind of the ~2885 ± 150 yr B.P. f5d p3.5 flow (Rubin et al., 1987; Moore and Clague, 1991) at around 600 m, from Hualalai, Hawaii (Wasklewicz, 1994). (E) Dissolution of the hornblende grain in the center is greater than the surrounding darker quartz and the bright magnetite grain in the lower left; from Clark Mountains, Marie Byrd Land, Antarctica. (F) Dissolution "etch" pattern on magnetite grain, from active crest of the Kelso Dunes, Mojave Desert, California. (G) Characteristic linear etching weathering pattern on clinopyroxene grain, from same site as D. (H) Biotite weathering by dissolution, from same site as 1B. (I) Biotite weathering by hydration and perhaps by the reprecipitation of bright iron-oxides, although it is possible that the oxides are primary. Sample from petroglyph adjacent to Stuart Mountain Dam, central Arizona.

The first part of this paper explains a niche that a microscopic approach may help fill, within the context of other methods of quantifying chemical weathering. The method and its limitations are detailed in the second part of the paper. Lastly, the measurement of in situ mineral dissolution is explored in case studies that exemplify four different types of research problems: (1) the initiation of a weathering form; (2) the maintenance of a weathering form; (3) the in situ measurement of mass lost from boul-

TABLE 1. DIFFERENT APPROACHES USED TO MEASURE RATES OF CHEMICAL WEATHERING

Approach	Method	Units	Change*	Selected citations
Catchment studies	Analyze output	t/acre/yr; Sr isotopes	W, E, A+, Tr.	Bricker et al., 1968; Mast et al., 1993; Blum et al., 1994
	Analyze output	mg/L; mol/m^2/yr	W, E, A+, Tr.	Dethier, 1986, 1988; Velbel, 1986, 1993a
	Field/lab coordinated studies	mol/m^2/yr	W, E, A+, Tr.	Swoboda-Colberg and Drever, 1993; Velbel, 1993b
	Mass balance-regolith formation	g/yr; kg/ha/yr	W, E, A+, Tr.	Pavich, 1986; Wakatsuki and Rasyidin, 1992
Analysis of soils	PROFILE model	eq/ha/yr	W, E, A+, Tr.	Sverdrup and Warfvinge, 1993
	Soil mass balance	Mass change	W, E, A+, Tr.	Merrits et al., 1992
	Physiochemical strain gauge	Strain, mass change	W, E, A+, Tr.	Brimhall and Dietrich, 1987
	Micromorphometrics	Volume change	W, E, A+, Tr.	Moran et al., 1988
	Soil characteristics	Changes in horizons	W, E, A+, Tr.	Birkeland, 1984; Mahaney, 1990
	Lithology comparison	Ratio surface/subsurface lithologies	W, E, Tr.	Birkeland, 1964
	Bedrock-to-soil with ^{10}Be	km/ma	W, E, A+, Tr.	Monaghan et al., 1992
Field measurements	Placed stone material	g/yr	W, E	Caine, 1979; Trudgill et al., 1994
	Micro-roughness meter	Slopes of microrelief	W, E	McCarrol and Nesje, 1993
	Microerosion meters	mm/yr	W, E	Viles and Trudgill, 1984
	Cone indentor	mm	W, Tr.	Hall, 1993
	Schmidt hammer	Rebound value	W, Tr.	Day and Goudie, 1977
	Compressional wave speeds	Velocity (km/s)	W, Tr.	Crook, 1986
	Ultrasound waves	Ratio	W, Tr.	Ilier, 1956
	Depth of weathering pits	Pit geometry	W, E	Fahey, 1986
	Differential grain relief	mm	W, E	McCarrol and Nesje, 1993
	Phenocryst and inclusion relief	mm	W, Tr.	Sharp, 1969
	Weathering rind thickness	mm	W, Tr.	Colman and Pierce, 1981
	Engineering description	Ordinal classes	W, E, Tr.	Dearman et al., 1978
	Weathering rind hardness	Ordinal classes	W, Tr.	Kiernan, 1990
	Pebble coherence	Ordinal classes	W, Tr.	Kiernan, 1990
	Boulder preservation	Boulder counts	W, E	Blackwelder, 1931
	Surface preservation	Removal of smooth surface	W, E	Sharp, 1969
	Clast splitting	Ratio split to non-split	W, E	Burke and Birkeland, 1979
	Mechanical strength	Ordinal classes	W, Tr.	Melton, 1965; Sharp, 1969
	Abrasion pH	pH	W, E, Tr.	Grant, 1969
Laboratory measurements	Stable oxide indices	Ratio of mobile to immobile oxide	W, Tr.	Reiche, 1945; Dixon et al., 1984
	Ratios to unweathered rock	g/g, ratio	W, Tr.	Jenny, 1941; Krauskopf, 1967
	Ratios to stable minerals	Ratio, for example to zircon	W, Tr.	Dryden and Dryden, 1946; Milnes & Fitzpatrick, 1989
	Mineral abundance over time	mol/cm^2/sec	W, Tr.	Blum et al., 1994
	Laboratory solutions	mol/m^3/yr	W, E	Swoboda-Colberg and Drever, 1993
	Quartz etching	Quartz characteristics	W, E	Lasaga and Blum, 1986; Tchakerian, 1991
	Calcite etching	Pit size distributions	W, E	MacInnis and Brantley, 1993
	Hornblende etching	μm/ka	W, E	Hall and Horn, 1993
	Thermoluminescence	Basalt weathering stages	W, Tr.	Ogelman and Kapur, 1983
	Clay mineralogy of weathering rind	Clay mineral types	W, Tr.	Kiernan, 1980; Colman, 1982
	K-Ar analysis of K-Mn oxides	Weathering ages in Ma	W, Tr.	Vasconcelos et al., 1992
	Transmission electron microscopy	Changes in micrographs	W, E	Eggleton, 1986
	Bone deterioration	Ordinal stages of weathering	W, Tr.	Lyman and Fox, 1989
	Compare ashes in different sites	Multiple characteristics	W, Tr.	Lowe, 1986
	Lead	Lead isotopes	W, Tr.	Erel et al., 1994
	Cosmogenic nuclides	Isotopic ratios, ages in Ma, k.y.	W, E	Gosse et al., 1993; Brown et al., 1994
	C and O isotopes	Laser profiles	W, A+	Aborg et al., 1993
Examination of dated features	Tombstones	mm/yr	W, E	Meierding, 1993a,b
	Buildings	mm/yr	W, E	Dragovich, 1986; Paradise, 1993
	Barrows	mm/yr	W, E	Goudie et al., 1990
	Historic emergent shorelines	mm/yr	W, E	Matsukura and Matsuoka, 1991
	Photography	mm/yr	W, E	Pentecost, 1991
	Rock art	Classes; percent art lost	W, E	Campbell, 1991; Benito et al., 1993

*W = weathering; E = erosion; A+ = addition of mass; Tr. = mineral transformations.

der weathering rinds over time; and (4) an assessment of the significance of temperature, precipitation, and microenvironment in the dissolution of plagioclase.

THE NEED FOR AN IN SITU MICROSCOPIC APPROACH

The last decade has seen considerable growth in the variety of methods (Table 1) used to quantify natural rates of chemical weathering (e.g., Colman and Dethier, 1986; Brimhall and Dietrich, 1987; Moran et al., 1988; Brimhall et al., 1991; Colin et al., 1992, 1993a; Drever and Zobrist, 1992; Steward, 1993; Velbel, 1993a, 1993b; Brown et al., 1994; Blum et al., 1994; Bluth and Kump, 1994; Lasaga et al., 1994). This growth is despite an inherent observational constraint that natural chemical weathering is often so slow as to be virtually unnoticeable during the career of an individual researcher (Colman and Dethier, 1986; Gosse et al., 1993; Beauvais and Colin, 1993; Brown et al., 1994).

Some of these new approaches have an integrative, holistic perspective that biochemical and physical weathering are synergistic, affect surficial materials that range in depth from micrometers to hundreds of meters, and span time scales up to 100 Ma (e.g., Brimhall et al., 1988; Vasconcellos et al., 1992; Colin et al., 1992, 1993b; Brown et al., 1994). This holistic perspective views weathering as more than just alteration of minerals; it relates weathering to authigenic minerals, mass fluxes in the regolith, soil development, biogeochemical interactions, petrography, and eolian additions and losses and hence impacts virtually all studies of natural weathering because of the ubiquity and the time depth involved in weathering (Brimhall et al., 1991; Lasaga et al., 1994; Pope et al., 1995).

Multiple techniques used in tandem have yielded new insights (e.g., Brimhall et al., 1991; Beauvais and Colin, 1993). For example, secondary electron images inform about three-dimensional "topographic" relationships between minerals. High-resolution transmission electron microscopy determines the nature of pores smaller than the 0.1 μm limit of the BSE method (Krinsley et al., 1993). The electron microprobe obtains quantitative chemical analyses. X-ray diffraction reveals mineralogy, and physiochemical strain-gauge data provide insight

into chemical gains and losses in larger systems (Brimhall et al., 1991).

Even with new perspectives and techniques, there is room for an in situ microscopic approach to help address the following two problems in the quantification of chemical weathering: chemical weathering of rocks is often indirectly measured, and different methods measure chemical weathering in units that are often noncomparable.

In many quantitative studies of chemical "weathering," the decay of minerals in a natural setting is only inferred by studying the erosion of weathered materials. Consider solutes leaving a drainage basin (April et al., 1986; Velbel, 1993b; Gibbs and Kump, 1994). Solutes provide data on loss of mass integrated over an area, but this is a combination of weathering, transportation, eolian input, and cation-exchange reactions (April et al., 1986; Cerling et al., 1989; Goudie et al., 1990) that varies over short time scales (Dethier, 1988). Similarly, traditional field-based approaches (Blackwelder, 1931) still in common use today rely on measuring the erosion of weathered material, for example, the morphometry of "weathering pits" (Berry, 1994). Even in measurements of the decay of historical monuments (Paradise, 1993) or tombstones (Meierding, 1993a, 1993b) weathering is inferred, because the rate of erosion is assumed to be limited only by the rate of weathering.

Where true chemical weathering has been measured in a natural setting, results from different methods are often not readily comparable. For example, the thickness of "weathering rinds" (Colman and Pierce, 1981) cannot be compared to hardness measured by the Schmidt hammer (McCarroll and Nesje, 1993), nor these to solutes (April et al., 1986), P-waves (Crook, 1986), changes in the geometry of weathering forms such as tafoni (Matsukura and Matsuoka, 1991), or strain (Brimhall and Dietrich, 1987). Problems of comparison are also encountered in relating field and laboratory studies of solutional erosion from weathering (e.g., Lasaga and Blum, 1986; Sverdrup and Warfvinge, 1993; Casey et al., 1993; Velbel, 1993a, 1993b; MacInnis and Brantley, 1993; Lasaga et al., 1994). It may be that the quantification of chemical weathering has not been standardized (Table 1), in part because of the complexity of the processes involved, but also because techniques of measuring weathering have different traditions in different disciplines. For example, Quaternary geology has developed its own peculiar ways of measuring weathering, as has geomorphology, watershed hydrology, soil science, engineering, and interdisciplinary efforts to interpret supergene minerals.

METHODS

Images formed by back-scattered electrons reveal variations in sample composition, since the yield is a function of average atomic number (Pye and Krinsley, 1984; Dilks and Graham, 1985). BSE images show varying elemental compositions within a polished sample, with lower atomic number regions appearing darker and higher atomic number regions appearing brighter. In contrast, secondary electrons provide information on sample topography and three-dimensional relationships among minerals (Bohor and Hughes, 1971).

As exemplified in Figure 1, different types of information can be obtained from BSE imagery of minerals: (1) when minerals are unweathered, at least at the scale of BSE imagery; (2) when minerals are partially or totally weathered to secondary products; and (3) porosity produced by dissolution of weathered minerals. Note the clear demarcation between the dissolved and unweathered orthoclase in Figure 1C and plagioclase in Figure 1D. Etched pyroxene can be differentiated from dark dissolution pores in Figure 1G. In contrast, secondary electrons cannot readily differentiate clays from weathered quartz in Figure 1A. BSE has also been useful in the rapid identification of heavy minerals (cf. Braun et al., 1990; Colin et al., 1992).

Porosity can be measured optically (Ehrlich et al., 1984), but BSE has the advantage of distinguishing much smaller pores, down to ~0.1 μm diameter (Krinsley et al., 1993). Furthermore, analysis of mineral composition by energy dispersive or wavelength dispersive detectors is routinely available on electron microscopes with back-scatter detectors. Although smaller pores can be resolved with secondary electrons, the digital output is not easily processed because edge effects make pore rims bright. Another advantage of BSE is the simultaneous imaging of texture and average atomic number (Milnes and Fitzpatrick, 1989; Cochran and Berner, 1993).

For this study, weathered rock was broken down into rock chips, which were placed in 2.5-cm-diameter molds filled with epoxy. One side of the weathering rind was polished, with the last stage a 0.3 μm aluminum grit. The following discussion presents the method of measuring porosity from digital image processing (DIP) of BSE imagery (Fig. 2).

(1) Obtain BSE Image. Image quality depends upon polish quality. Whether the output is photographic (as here) or digital, there must be enough contrast to differentiate materials.

(2) Video Digitizing. Newer electron microscopes often provide digital data for subsequent image processing. However, to demonstrate the utility of the technique for researchers who do not have access to digital BSE output, black-and-white prints of images from a JEOL™ Superprobe were video digitized into a PC-based image processing system. In this case ERDAS software and a Sony camera were used to make analog-to-digital conversions of gray-scale BSE images into digital imagery on a scale of 256 (0 to 255) in a one-band 512 × 512 matrix (Jensen, 1986). A "control" image was used at the start and end of each video-digitizing session to verify that results would be comparable. Specialized photo-stand light bulbs were used originally, but a gradual deterioration occurred that caused differences in results between sessions. Then, inexpensive household bulbs were tried, and results were repeatable from session to session.

(3) Data Preprocessing. Each specific BSE image has material unsuitable for measurement of pores with DIP. Epoxy, magnification and scale information, borders, and vesicles in basalt were "cut out." Biotite was also cut out for reasons discussed later. The resultant image was processed further.

(4) Isolation of Weathered Material. The focus of this paper is the measurement of pores from in situ chemical dissolution. However, BSE can also be used to "map" and measure secondary products, because they have different elemental compositions and textures than primary minerals (Figs. 1B and 1G). In some cases, the Laplacian filter (cf. Jensen, 1986),

$$\text{Mask} = \begin{matrix} 0 & -1 & 0 \\ -1 & 5 & -1 \\ 0 & -1 & 0 \end{matrix}$$

had the effect of bringing out weathered zones. After recognition in unenhanced or enhanced images, pixels in weathered areas were tabulated as they were "cut out." In order to preserve data as to original mineralogy, different weathered areas are assigned different "classes."

(5) Classification. Histograms of the remaining data revealed specific peaks of

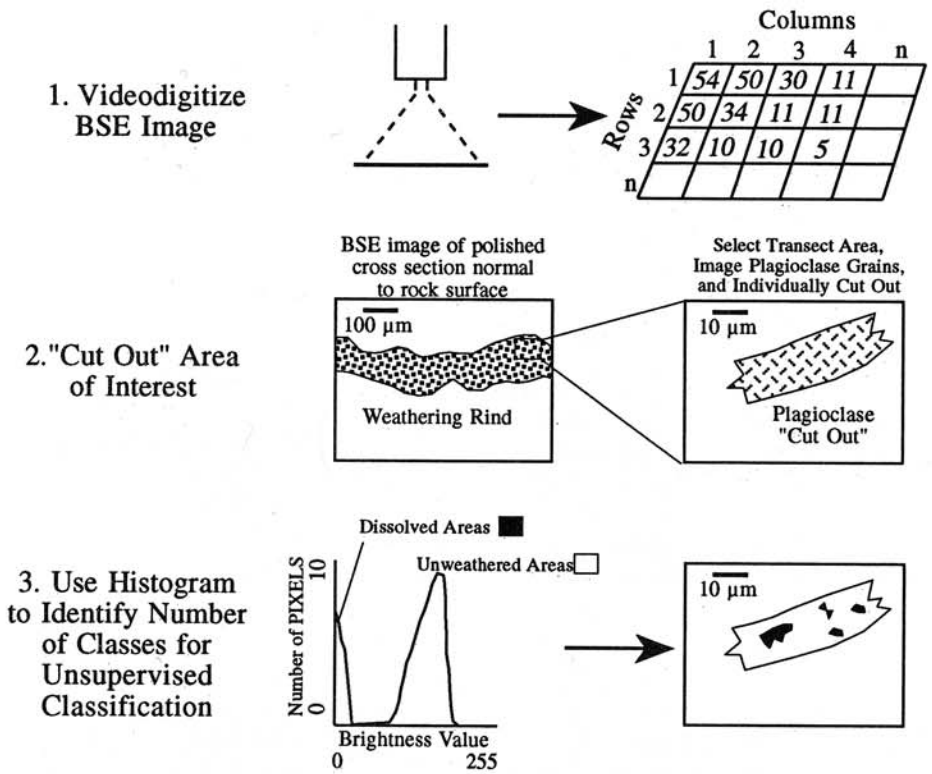

Figure 2. Generalized diagram illustrating digital image processing of back-scattered electron images to obtain data on percent of a mineral, in this case plagioclase, that has dissolved.

gray-scale values representative of different minerals and porosity. Histograms were used to identify the number of classes in the unsupervised classification of the remaining data (Jensen, 1986). The output from the ERDAS image processing program is a "map" of the different classes of brightness values and the number of pixels in each class. With scale information about pixel area, these data are translated into cross-sectional area in square micrometers. Then, square micrometers can be readily translated to a variety of units, for example g/m^2 with knowledge of sample density.

This method of assessing porosity has several limitations.

(1) Scale Effects. Porosity can be finer in resolution (Nahon, 1991) than the ~0.1 μm limit of BSE (Krinsley et al., 1993). Internal pores in clay matrices, for example, are best imaged by high-resolution transmission electron microscopy (Robert and Tessier, 1992). Therefore, porosity measured by BSE is best interpreted as a minimum value.

Pores greater than ~0.1 μm diameter are measured differently at different magnifications in the same sample area (Fig. 3). For example, Figure 1H appeared to be an image of solid biotite, until dissolved areas were resolved at higher magnifications. An efficient strategy is to use the lowest magnification that can resolve the smallest porosity visible with BSE. For example, "plateau" is sometimes reached (Fig. 3A), where it is more efficient to use a lower magnification to analyze a larger area. In other cases (Fig. 3B), higher magnifications are necessary to resolve pores. In this study, variable magnifications from 400× to 5000× were applied.

(2) Misidentification of Weathering. A second limitation of BSE includes the potential to incorrectly identify and interpret weathered minerals, unweathered minerals, and pore space. This section explores how these problems were identified and handled.

Sometimes organic matter occupies pores in weathering rinds (Cochran and Berner, 1993) but is dark in BSE imagery because of the low atomic number. The presence of carbon can be tested with a wavelength dispersive detector and by switching back and forth between secondary (organics visible) and back-scattered electrons (organics dark) (Watts, 1985).

Porosity occurs in primary rocks and minerals. Basalt contains vesicles, and even unweathered quartz can contain 0.21% to 0.51% voids in 10–50 nm pores (Shur et al., 1966). Porosity can also be "inherited" from a prior weathering cycle or from diagenesis (Giles and Marshall 1986; Ehrlich et al., 1984, 1991), or from millions of years of subsurface weathering (Vasconcelos et al., 1992). How porosity data is interpreted depends upon the field context. In the case study on alveoli, inheritance from a prior weathering cycle is likely. In the case of polygonal cracks and gnamma pits, some pores were likely inherited from a time when the current surface was lower in the weathering rind. Rates of dissolution cannot be determined where there is uncertainty over when weathering started. In the first two case studies, however, the issue is not the rate of weathering but relationships be-

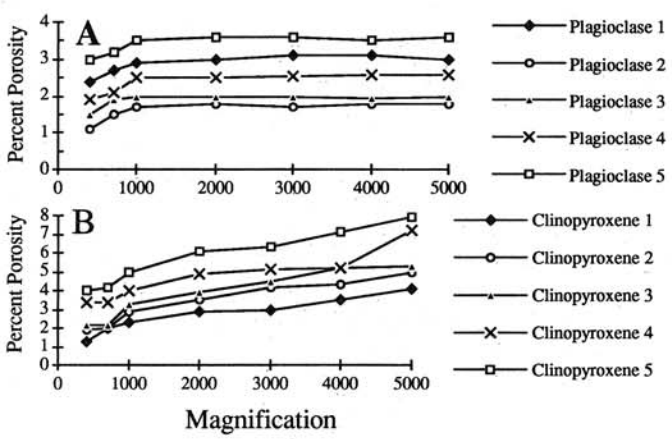

Figure 3. Plot of porosity versus magnification for (A) plagioclase and (B) clinopyroxene from f5d p3.5 flow Hualalai, Hawaii (Moore and Clague, 1991). In each mineral curve, the same area was analyzed.

tween contemporary weathering forms and total porosity, regardless of when it occurred.

Studies of weathering rates over time, in contrast, must assume that the "weathering clock" starts at a known time with a value that can be established. In the third case study of weathering rind development on ventifacts, the weathering system was "reset" by eolian abrasion. This was verified by examining the rock well below the measured rind, and pores ≥0.1 μm could not be discerned. Inherited porosity was similarly ruled out in the fourth study on Hawaiian plagioclase weathering, because pores could not be seen within plagioclase grains in the interior of the basalt, at least at the 0.1 μm resolution limit of BSE.

It is difficult to measure porosity in supergene products such as clay minerals because of internal porosity (Robert and Tessier, 1992). Although secondary precipitates were not observed within weathering pores studied here, they would pose complications (Brimhall et al., 1988; Merino et al., 1993). After recognition with EDS (energy dispersive spectrometry) or TEM (transmission electron microscopy), they could be manually cut out of the digital image to avoid influencing results.

Mineral weathering, however, cannot always be identified with BSE. For example, quartz weathers to an amorphous phase before it subsequently dissolves (Pope, 1995). Such processes may also occur in other silicates (Schott and Petit, 1987). These amorphous areas are not distinguishable from quartz using BSE alone because there is no change in atomic number or texture. Yet, when barium adsorbs to amorphous zones on quartz, weathered areas appear brighter and distinguishable by BSE (Fig. 1B).

In summary, porosity values cannot be used blindly without consideration of the inherent limitations of the imaging system or the field context.

(3) Expansion Effects. For minerals that expand when weathered, such as biotite (Fig. 1I), it is difficult to make a direct translation between porosity and loss of mass. Although biotite expansion can be very important in weathering dynamics, pores created by physical expansion alone would not represent a loss of mass. Because it is not possible to discern dissolution pores from physical expansion, the biotite that was present in the aplite ventifact case study (<4% by area) was cut out before further analysis took place; therefore, the measured rate of dissolution in the third case study excludes loss of mass from biotite.

(4) Sample Preparation. Sample pretreatment can mimic weathering effects. Additional pitting and coatings can form as samples are prepared for SEM examination (Cremeens et al., 1987). Polishing can create shallow scars, and crack enlargement can occur with larger grits. As a consequence, only distilled water and ultrasonic cleaning were used in the preparation of cross sections. Grooves and shallow pits, created by the submicron aluminum polishing grit, do not affect BSE imagery—although they can be seen when secondary electrons image the same locale. Thus, using both techniques it is possible to determine the difference between pitting made by polishing and natural dissolution.

INITIATION OF ALVEOLI IN CENTRAL ARIZONA[1]

Tafoni and alveoli are large and small honeycombed hollows in rocks, where enlargement by grain erosion is limited by weathering. Matrix and grain-boundary dissolution, salt-expansion weathering, rock coatings, differential fluid flow toward rock surfaces that are not coated, expansion of clays, silica dissolution assisted by salt and organic acids, and ferrous iron reactions may play a role in the *extension* of caverns by promoting granular disintegration of rock (e.g., Dragovich, 1969; Conca and Rossman, 1982; Mustoe, 1982; Twidale, 1982; McGreevy and Smith, 1984; Conca and Astor, 1987; Matsukura and Matsuoka, 1991; Young and Young, 1992; Paradise, 1993; Mottershead and Pye, 1994). An uncertainty exists in research on honeycombed weathering forms about how they *start*.

This case study examines whether porosity is associated with *initiation* of the smallest hollows (subcentimeter alveoli). Samples were collected from sandstones of the Supai formation, near Sedona in central Arizona, where calcium carbonate, amorphous silica, and clay minerals cement quartz grains. Forty-five samples were collected from transects into and out of alveoli smaller than a centimeter. Fifteen samples came from the center of alveoli; fifteen from on the sides; and fifteen from 1 cm away from alveoli. Porosity was measured within 100 μm of the surface.

Samples from the centers, sides, and distant from alveoli had porosity values that are significantly different from one another (p [probability] < .01). Alveoli centers averaged (and 1 S.D.) a porosity of 47.9% ± 13.5%, alveoli sides 21.7% ± 11.6%, and locations 1 cm distant from alveoli 9.4% ± 5.0%. Porosity measurements of sandstone 5 mm beneath alveoli centers had values of 4.6% ± 3.0%. Higher porosity in the center and sides of incipient alveoli, however, only reveal a correlation between form initiation and weathering. An advantage of BSE imagery is an ability to examine in situ evidence for different weathering processes.

Qualitative observations of BSE imagery (Fig. 4) indicate that matrix removal is the most important process in alveoli initiation. Figure 4B reveals an alveolus where all but a few remnants of silica and clay cement have been lost. Most of the calcium carbonate (brighter in image) cement in Figure 4D has eroded. Figure 4C illustrates clay loss in the center of an alveolus. The ragged edges of quartz in Figures 4D and 4F suggest that weathering has occurred along grain margins, but the most-weathered quartz grain only had a porosity of 2.3%.

A model of tafoni initiation consistent with these data starts with enough matrix loss to reduce intergrain cohesion. Incipient alveoli occur where there is a total porosity within 100 μm of the rock surface >~32%. Upon reaching this threshold of porosity, granular disintegration occurs. Detached quartz grains are then eroded by transport processes involving lichens (Fig. 4E), and by inference, probably mass wasting, overland flow, and perhaps deflation. The threshold needed to reduce resistance to shear stresses enough to erode grains will likely be different for each lithology.

This study is the first to define a threshold associated with the initiation of alveoli. A lithologic, climatic, or spatial pattern may become evident with additional data on incipient alveoli in other settings. This case study also illustrates how a microscopic approach measures weathering in situ, as opposed to measuring the morphometry of a form that is a product of both weathering and erosion of weathered material.

[1]GSA Data Repository item 9519, data on the case studies, is available on request from Documents Secretary, GSA, P.O. Box 9140, Boulder, CO 80301.

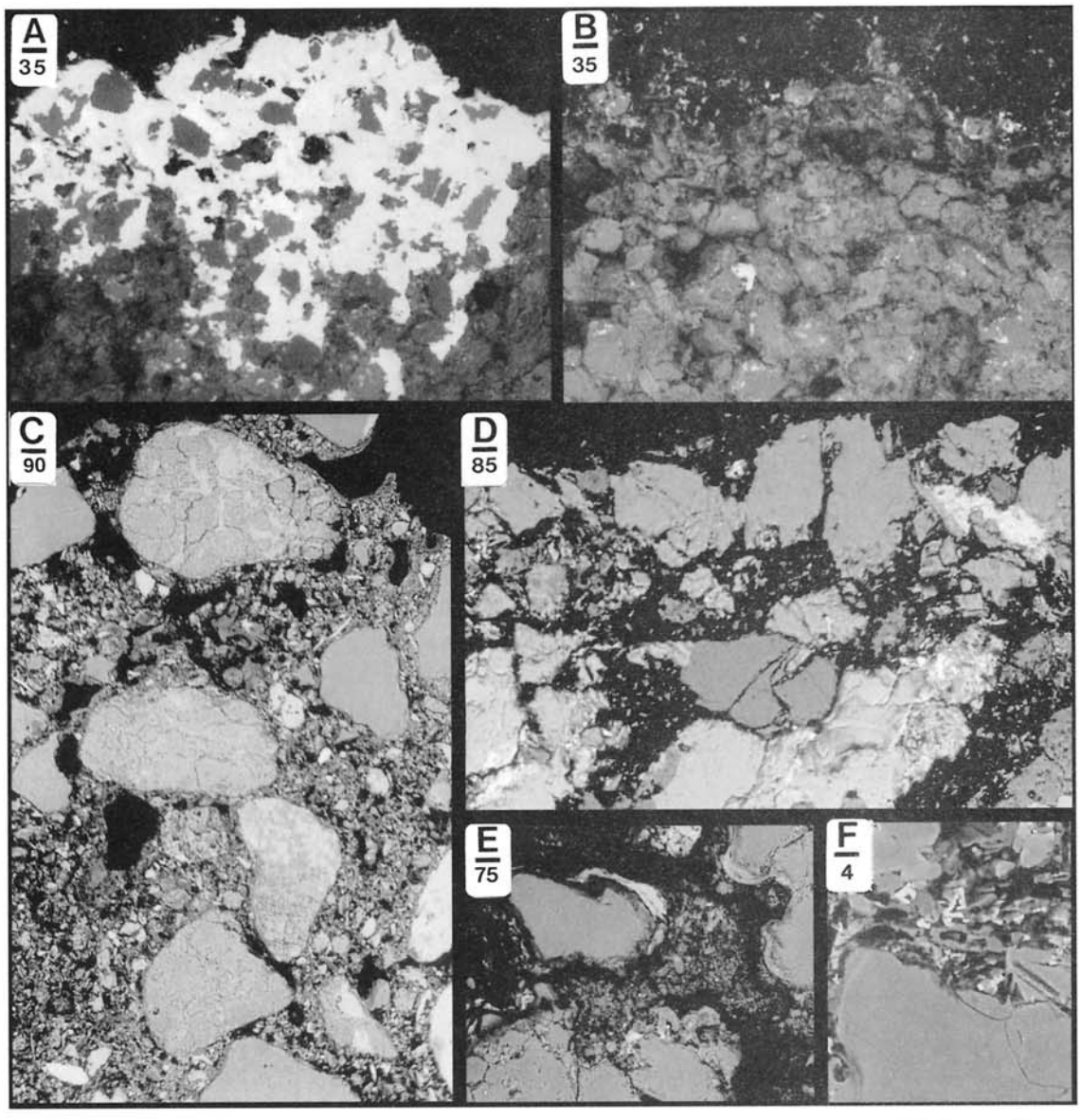

Figure 4. BSE views of alveoli development in the Sedona area of Arizona. Scale bar in micrometers. (A) Manganiferous rock varnish (brighter material, analyzed by EDS) cementing quartz grains in a sample immediately adjacent to an incipient alveolus. (B) Alveolus pit, where matrix is silica and clay minerals. (C) Alveolus pit, where matrix is clay minerals. Greater porosity occurs in upper left section, which is at the center of the alveolus. The loss of matrix drops off rapidly away from the pit center, to the lower right. (D) Alveolus pit, where the brighter matrix cement is $CaCO_3$, which appears to be lost through dissolution. (E) Alveolus pit less than a millimeter deep is starting through lichen weathering. The speckled pattern surrounding the apparently detached quartz grain is calcium oxalate—part of a lichen thallus that is mechanically separating the grain. (F) Close-up of Figure 4D, where the edges of quartz grains are undergoing dissolution.

MAINTENANCE OF POLYGONAL CRACKS AND GNAMMA PITS IN BASALT

Processes that initiate a weathering form may differ from those that foster its maintenance. A positive feedback must occur for a form to grow. A negative feedback erases the form. A dynamic equilibrium results in form maintenance. This case study examines in situ mineral dissolution and rock coatings associated with gnamma pits and polygonal cracks; the objective is to understand how these forms continue to exist.

Polygonal cracks and gnamma pits develop on basalt boulders on the drier slopes of Kaho'olawe and Maui islands in Hawaii. For this study, a single boulder (Fig. 5) was sampled from a hillcrest near Pu'u Hipa (~280 m) on the west side of Maui. The boulder has an orange-brown glaze of mostly amorphous silica (Farr and Adams, 1984; Curtiss et al., 1985), as well as patches of manganiferous rock varnish (Dorn et al., 1992). Coatings of silica glaze also occur on sandstones that are polygonally cracked (Williams and Robinson, 1989). The particular boulder (Fig. 5) was selected for study because I saw a platelet (5 mm × 3 mm × <1 mm; Fig. 6A) erode during an intense

Figure 5. Polygonal cracking and gnamma pitting of surface of olivine basalt boulder, Maui, Hawaii.

rain event. The platelet had a porosity of 37%. Figure 6E presents the new surface of the boulder that was sampled after the spalling event.

On the boulder, polygonal cracks sometimes occurred at preexisting fractures (cf. Whalley et al., 1982). The greater porosity in the center of Figure 6G, for example, is associated with a microfracture that runs downward at least 4 mm into the rock. In contrast, there is no clear correspondence between gnamma pits and observable lithologic weaknesses. Lichens, cyanobacteria, and fungi are more common in gnamma and crack depressions; they erode rock varnish and enhance rock dissolution rates (cf. Wasklewicz, 1994), as seen on the right side of Figure 6F. The focus here, however, is not how the weathering forms started, but how they continue to exist. Maintenance requires that weathering and erosion of pits and cracks be greater than (or equal to) weathering and erosion of interpit "ridges."

The role of mineral dissolution and silica glaze in the maintenance of gnamma pits and polygonal cracks was assessed through ninety BSE images. Porosity was measured in the upper 40 μm of the weathering rind; silica glaze thickness was also measured above the rinds. Three images each were analyzed from ten samples of polygonal cracks; three each from ten samples of gnamma pits; and three each from ten samples of "interpit" ridges. In addition, each section was imaged 5 mm under rinds to assess porosity prior to subaerial exposure.

Figure 7 reveals that porosity increases with silica glaze thickness, a relationship that was significant at $p < 0.001$. Similar correlations were found when the data set was divided into gnamma pits, polygonal cracks, and interpit locales.[2] Some of the scatter could be from the inability of this method to measure pores smaller than 0.1 μm. Another problem is that it was not possible to distinguish primary vesicles from dissolved areas; therefore measured values undoubtedly include some of the inherent vesicle porosity in the boulder. Interior porosity 5 mm beneath rinds measured 2.9% ± 2.3%, a low value that may suggest the boulder originated in an interior portion of a lava flow.

A conceptual model for the maintenance of gnamma pits and polygonal cracks could be described as a see-saw between increasing rind weathering porosity and the development of rock coatings. The silica glaze rock coating (and to a lesser extent rock varnish) holds the weathering basalt in place as porosity increases (Fig. 6H, left side of Fig. 6F, right side of Fig. 6D). Porosity increases until erosional shear stresses are greater than interparticle resistance to shearing, and erosion of rind and rock coating occurs. No weathering rind exceeded a porosity of ~47% (Fig. 7), whereas rind spalling was observed to occur at a porosity of ~37%.

In this model, erosion is episodic, occurring when the "case hardening" effect of the coating can no longer hold together a rock surface weakened by weathering. After a weathering rind spalls, incipient coatings may form on the new subaerial surface (Fig. 6B). This new surface may also spall away again (Fig. 6C), until a point is reached where a rock coating can thicken on a relatively stable basaltic substrate (Fig. 6H). Figure 6D shows the center of a polygonal crack (left side) and the side of the crack (right side), where the lack of a rock coating on the left side indicates ongoing spalling of the rind.

This case study builds on three themes in weathering: Silica glaze enhances the stability of rock surfaces (Hobbs, 1917); rock coatings are important in the maintenance of weathering forms (e.g., Conca and Rossman, 1982; Conca and Astor, 1987; Williams and Robinson, 1989; Mottershead and Pye, 1994); and, lastly, weathering in the immediate or distant past influences the current form of the land surface (cf. Twidale, 1982; Brimhall et al., 1991; Vasconcelos et al., 1992; Gosse et al., 1993). This case also illustrates that the amount of chemical weathering (measured here as in situ porosity) may not necessarily relate to the current shape of a weathering form, an assumption made by some who try to infer rates of weathering by measuring form (Table 1). The amount of in situ weathering, in this case, depends upon the current state of dynamic equilibrium between chemical weathering, rock coating formation, and shear stresses.

MEASUREMENT OF WEATHERING RINDS ON GLACIAL VENTIFACTS

The first two case studies concerned how measurements of in situ weathering can reveal insights into the initiation and maintenance of weathering forms. This case study turns to how digital processing of BSE imagery can be used to quantify rates of in situ dissolution, and to compare units commonly used to measure weathering that are not now comparable. Rates of in situ dissolution can only be determined where physical erosion can be ruled out, lithological and present-day microenvironmental fac-

[2]Data appear in the GSA Data Repository. See footnote 1.

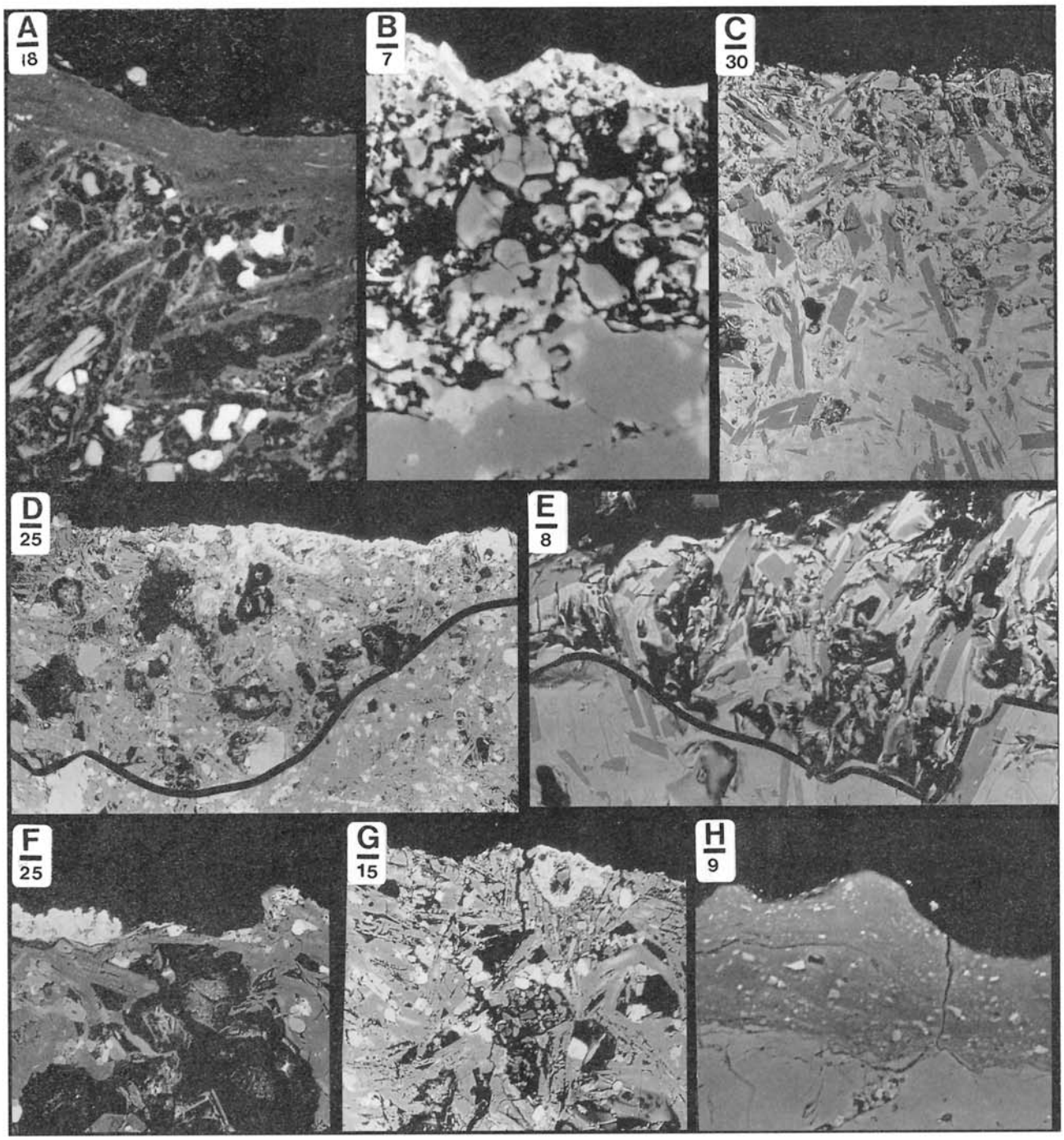

Figure 6. BSE imagery of weathering associated with polygonal cracking and gnamma pitting of basalt from Maui Island, Hawaii. Scale bar in micrometers. Images A, B, C, and E are from gnamma pits. Images D, F, and G are from polygonal cracks. Image H is from an "interpit" locale. The lines in D and E denote the base of the weathering rind. Silica glazes occur on top of the weathering rinds in images A and H. Rock varnishes occur in images B, D, and F and are distinguished by brighter textures (from higher Z [atomic number] of Mn and Fe). Lichen growth, not visible with BSE (Watts, 1985), occurs on the right side of F.

tors are controlled as much as possible, and inherited weathering is unlikely.

Bach (1995) presents a situation where long-term rates of subaerial boulder weathering can be studied. The Pleistocene glacier at Bishop Creek periodically advanced out of the Sierra Nevada, California. Corresponding katabatic winds polished morainal boulders into ventifacts with characteristic grooving. As the glacier terminus shifted positions, the location of eolian abrasion shifted in a fashion summarized in Figure 8. Eolian abrasion ceased at position V1 about 60–65 ka. Abrasion ceased by ~17 ka at V2 and ~14 ka at V3 (Bach, 1995). Of the boul-

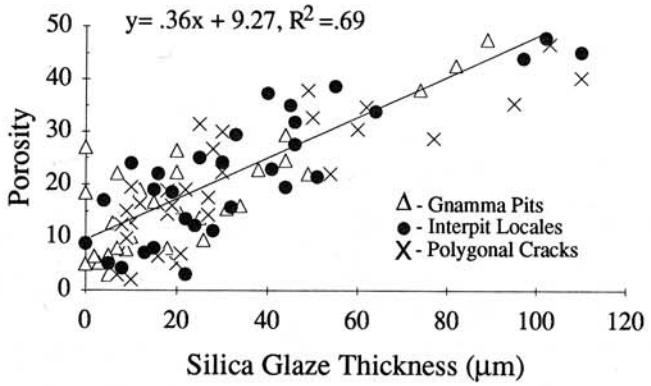

Figure 7. Scatter plot and linear regression of porosity in the upper 40 μm of the weathering rind on basalt boulder in Figure 5, plotted against silica glaze thickness immediately above the weathering rind.

ders that showed grooving, most had lost 5%–95% of their windward abraded surfaces to spalling. Where eolian polish is still present, however, only chemical weathering and no mechanical loss has occurred since abrasion ceased.

The amount of weathering that predated eolian abrasion was assessed by examining porosity in the rock at a depth of 1.5 cm under the weathering rind. No inherited porosity was found to the 0.1 μm limit of the BSE method. Microenvironment was controlled by avoiding lichens and collecting from the tops of the boulders in order to minimize the influence of water runoff and water retention that can amplify weathering rates (Fig. 9, D and E). In order to control lithology, only aplite samples were used (Fig. 9, A, C, D, and E), not other rock types at the site (Fig. 9, B and F). Rinds were measured from nine different aplite boulders from sites V1, V2, and V3 (Fig. 8).

A traditional approach to the study of weathering rinds is to measure rind thickness. Using BSE imagery, rind thicknesses averaged 0.9 mm with a standard deviation of 0.5 mm on nine aplite ventifacts from site V3; this is statistically indistinguishable from the nine ventifacts from site V2 (1.1 ± 0.6 mm). In contrast, nine aplite ventifacts from site V1 had a statistically distinct ($p < 0.01$) population of rinds at 3.2 ± 1.4 mm. Rind thickness appears to develop at a fairly linear rate of ~0.5–0.6 mm/k.y. for this rock type and environment.

The same BSE imagery used to make rind thickness measurements was used to calculate porosity.[3] The loss of mass from dissolution was calculated from density of aplite (~2.6 g/cm^3), rind thickness (mm), rind porosity (%), and time since eolian abrasion ceased (k.y.). Sites V1 and V2 (late Wisconsinan) dissolved at 40 ± 16 g/m^2/k.y. and 43 ± 16 g/m^2/k.y., respectively. In contrast, the long-term average at site V3 (early Wisconsinan) jumped to 67 ± 23 g/m^2/k.y. (Note that these values are minimums, because they exclude pores <0.1 μm and loss of mass from biotite, which composes <4% of the aplite).

The rate of porosity growth through dissolution appears to increase over time, which is consistent with Meierding (1993b, p. 283), who also found that subaerial weathering accelerates over time. A positive feedback is explained by retaining more water as more capillary pores develop (Swoboda-Colberg and Drever, 1993). These results differ from studies of mafic soil clasts, where rates of rind thickening slow over time (Colman and Pierce, 1981). The difference in results could be due to progressive spalling of older weathering rinds within soil, which would give the impression that rates of weathering slow over time. Another possibility could be that the pore sizes in aplite (Fig. 9) have slower rates of evaporation and capillary water movement than the mafic clasts of Colman and Pierce (1981).

[3]Porosity data for each boulder are presented in the GSA Data Repository. See footnote 1.

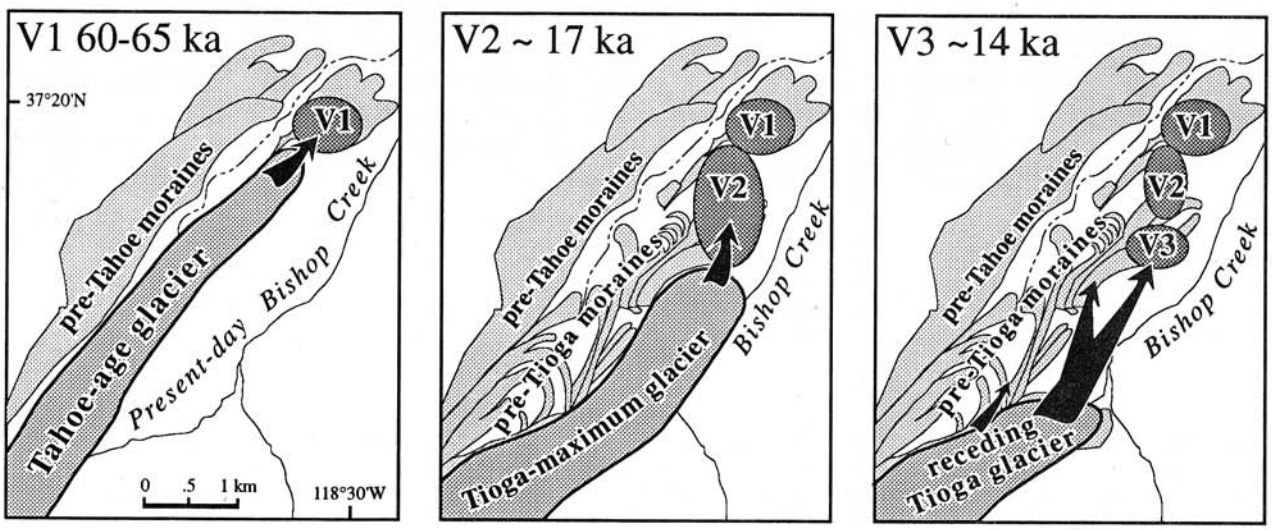

Figure 8. Ventifact sampling areas at Bishop Creek, eastern California (modified from Bach, 1995).

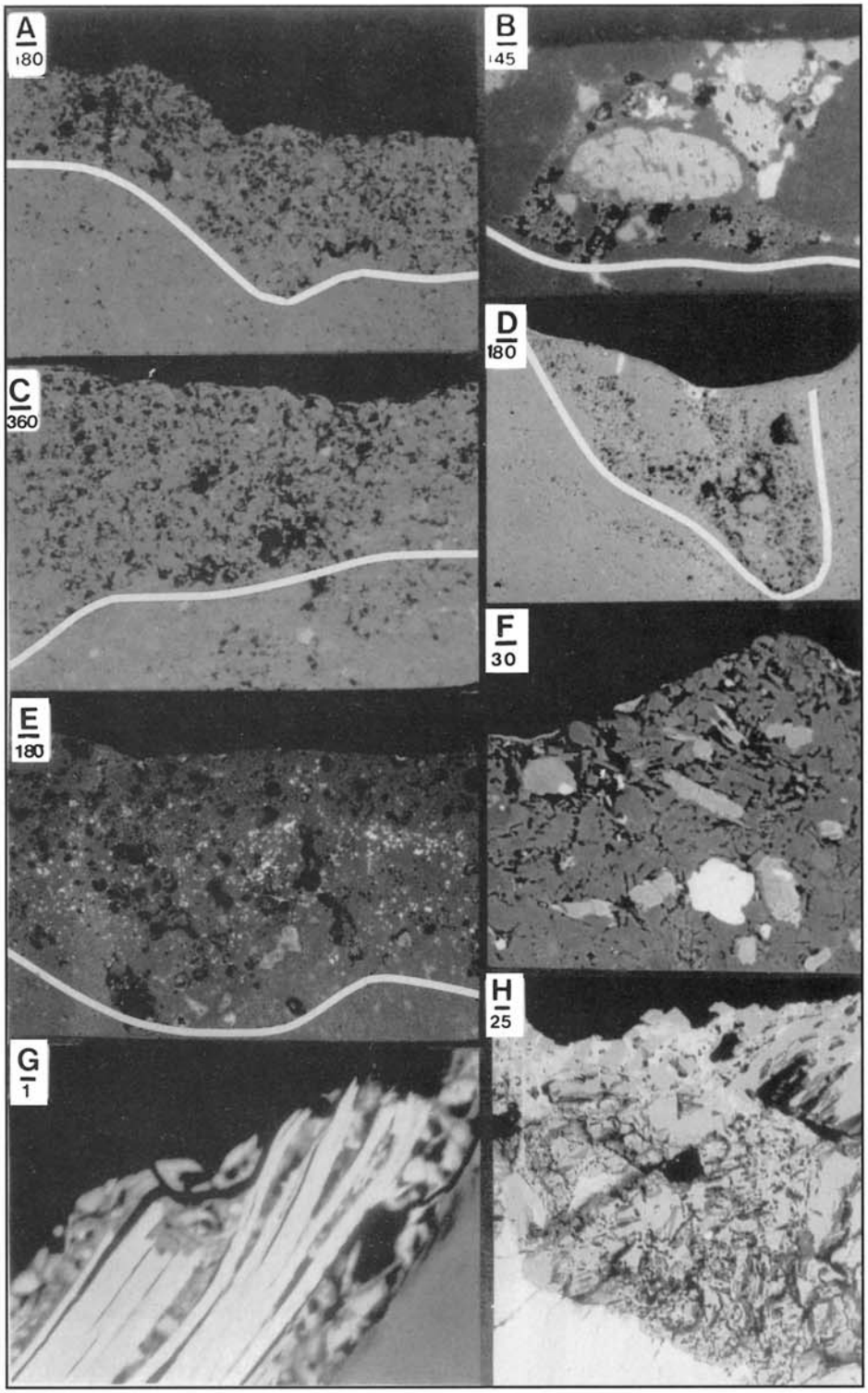

Figure 9. BSE imagery of weathering rinds associated with ventifacts sampling areas at Bishop Creek. Scale bars in micrometers. (A) From site V2. (B) From site V3, but a slightly different lithology that was not comparable to the other samples. (C) From site V1. (D) From site V3, but from a locale where water collects in a depression. (E) From the same boulder as Figure 9A, but from a position 15 cm into the soil that was excavated. (F) From site V2, but an andesite boulder that has a different style and abundance of pore development. (G, H) From the same boulder as Figure 9A, but from a section where the ventifact surface has eroded. In places, the granular erosion has been halted by silica glaze or rock varnish. Silica glaze can be seen encapsulating biotite in G, and bright rock varnish holds the very surface of the plagioclase together in H.

This case study illustrates how a microscopic approach can be used to "translate" different units that are used to measure weathering. The thickness of a weathering rind (in millimeters) is a classic field measure of site-specific weathering (e.g., Colman and Pierce, 1981; Birkeland, 1984; Berry, 1994). Rinds are visible in part because of dissolution, which creates porosity. Where indirect measures of weathering are from loss of mass, the resultant porosity can be measured in situ and compared with studies of catchment weathering (e.g., Velbel, 1993a) or soils (e.g., Brimhall et al., 1991; Colin et al., 1992; Sverdrup and Warfvinge, 1993).

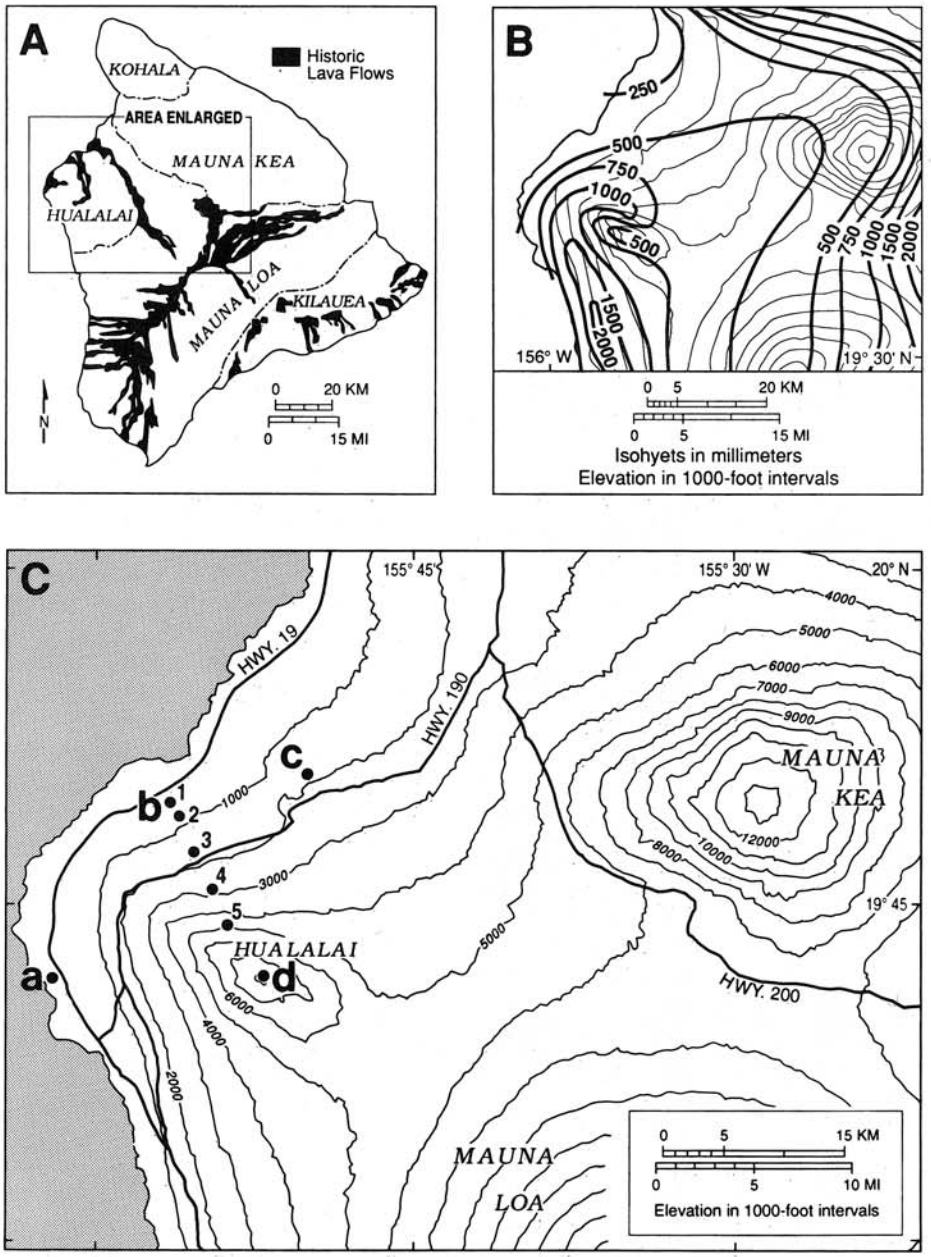

Figure 10. Maps of collection sites on Hualalai Volcano, Hawaii. A. Lava flow data from Moore et al. (1987). B. Precipitation information from Giambelluca et al. (1986). C. Numbers identify collection locales on ~2885 ± 150 yr B.P. flow f5d p3.5 (Rubin et al., 1987; Moore and Clague, 1991), and letters identify sites on ~2- to 3-k.y.-old lava flows sampled along a 500 mm isohyet.

TEMPERATURE, PRECIPITATION, AND MICROENVIRONMENT IN PLAGIOCLASE DISSOLUTION

Climate is generally perceived to be a key variable in chemical weathering (cf. Yatsu, 1988; Nahon, 1991; Bluth and Kump, 1994). Quantifying climatic controls, however, has been difficult (Pope et al., 1995). In this case study, digital processing of BSE imagery of Hawaiian basalts is used to assess the role of mean annual temperature, mean annual precipitation, and microenvironment on plagioclase dissolution. Hawaii "provides a unique opportunity to study, side by side, rocks of similar composition that have been exposed to subaerial weathering for vastly different lengths of time. . . . Furthermore, the wide variations in topography and rainfall make it possible to assess how these factors affect rock weathering" (Farr and Adams, 1984, p. 1077).

Hualalai Volcano (Moore et al., 1987; Moore and Clague, 1991) offers a site where time, lithology, microenvironment, and climate can be controlled. Dominant lavas are alkaline olivine basalts (Clague et al., 1980; Moore et al., 1987), many of which have ^{14}C ages on burned charcoal (Rubin et al., 1987). Over 90% of Hualalai's surface is Holocene, with over half being younger than 3000 ^{14}C yr old. The advantage of this youth is the retention of constructional surfaces that permit a specific age assignment for the onset of weathering. Although lava flows usually lose their initial glassy surface within a few years (Farr and Adams, 1984), extensive sections of both pahoehoe and aa flows on Hualalai retain vesicular constructive surfaces for 10^4 yr (Kurz et al., 1990; Dorn et al., 1992).

Two studies were conducted to examine the interplay of precipitation, temperature, and microenvironment. First, a single lava flow was sampled along a moisture-temperature gradient from dry-warm conditions near sea level to wet-cool higher on Hualalai. Second, different lava flows of similar age were sampled along the 500 mm isohyet, allowing precipitation to remain constant while temperature varies with elevation (Fig. 10).

Three assumptions are made in both studies. First, prior to exposure in a weathering rind, pores do not exist in the matrix plagioclase grains. This assumption was tested and verified by examining nonphenocryst plagioclase grains at a depth of ~1 cm under the weathering rind. Pores were not observed at the ~0.1 μm limit of the BSE method.

Second, it is possible to control microenvironmental effects at the millimeter scale through careful sampling. Wasklewicz (1994) distinguished three very different weathering microenvironments on Hualalai. One is rich in organic acids released by lichens and other rock-surface organisms (Figs. 11A and 11B). Field-based studies of tropical basalt weathering (Schirrmeister and Störr, 1994; Wasklewicz, 1994) and laboratory studies (Welch and Ullman, 1993) have established that organic acids can greatly enhance weathering rates and can change weathering sequences in tropical settings. The second microenvironment is where rock coatings cover rock surfaces (Fig. 11C). The third microenvironment has

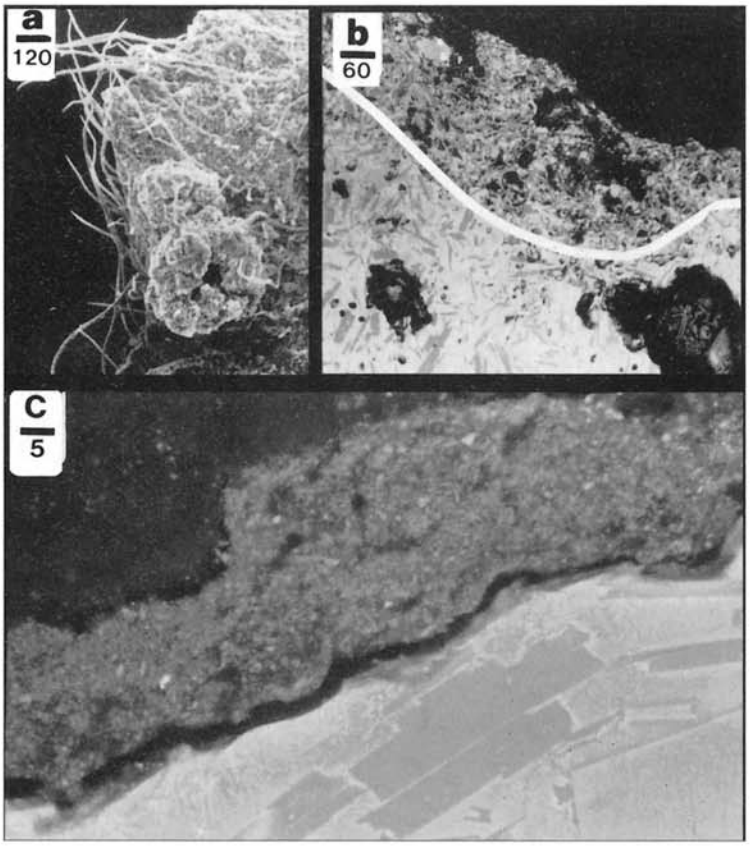

Figure 11. Different weathering microenvironments on Hualalai. Scale bars in micrometers. (a) Secondary electron image of lichen fruiting bodies with fungal hyphae at the surface of the 1800 A.D. Kaupulehu flow at 1113 m. (b) BSE image of the cross section of the weathering rind directly underneath the lichen in a.. The enhanced weathering zone, above the line, is the weathering rind of greater porosity. Large pores below the line are vesicles, which are cut out and not calculated in the image processing. (c) BSE view 70 cm distant from where a and b were imaged, only and underneath silica glaze (electron microprobe analysis of silica glaze: Na_2O, 0.74; MgO, 0.95; Al_2O_3, 13.21; SiO_2, 65.34; K_2O, 0.72; CaO, 1.75; TiO_2, 1.23; MnO, 0.03; FeO, 5.35). The darker minerals are plagioclase; note they lack pores at this magnification.

a paucity of acid-producing surface organisms and is not covered by rock coatings. Weathering of silicates in these organic-poor environments is primarily through reactions with carbonic acid, where "chemical weathering is severely limited because introduction of acids to the profiles is limited by rainfall" (Nesbitt and Wilson, 1993, p. 771).

In the first study, measurements were taken from both organic-poor and organic-rich microsites. Organic-rich environments were sampled directly underneath crustose lichens. Organic-poor environments were sampled ~3 mm distant from the margin of the rock coatings. In the second study, measurements were taken only from organic-poor microsites. Although it is impossible to normalize all microenvironmental conditions, due to environmental changes over the last 3 k.y., in my opinion this approach offers a reasonable partial solution to the very sticky problem of controlling microsite variability.

The third assumption is that plagioclase weathers by congruent dissolution. The larger phenocrysts of plagioclase on Hualalai weather by congruent dissolution, as well as the formation of clay mineral secondary weathering products (Wasklewicz, 1994). The smaller plagioclase grains within basalt matrix weather only by dissolution-making "holes" (Fig. 12). Clay minerals are not seen in these pores. Although the reason for this dichotomy is unclear, the "style" of weathering of the matrix plagioclase is to make holes. Our observations mirror those of Wasklewicz (1994), who also worked on Hualalai.

In each study, five different polished cross sections were examined with BSE from each site (Fig. 10). In each cross section, transects were placed in the upper 50 μm of the weathering rinds. The plagioclase feldspars encountered in the cross sections had a similar microprobe composition (Na_2O, ~3.5%; MgO, ~0.3%; Al_2O_3, ~29%; SiO_2, ~49%; K_2O, 0.3%; CaO, ~17; TiO_2, ~0.2; FeO, ~0.7), but energy dispersive analysis was used to verify the relative abundance of Na and Ca. The first 20 plagioclase feldspars (not including phenocrysts) with a CaO/Na_2O ratio of ~4–5 were selected for digital image processing. Images of individual plagioclase grains were then cut out with the ERDAS image processing system.

I assume that dissolution, totaled for 20 grains each from five separate samples from each site, is truly representative of the general state of the feldspars—not an artifact of some spatial anomaly in crystalline defects or lava flow character (White and Hochella, 1992). Natural weathering is known to be spatially discontinuous (Swoboda-Colberg and Drever, 1993; Wasklewicz, 1994), and not all grains that were in the transect were weathered (Fig. 12A). This is not surprising, because dissolution is preferential to crystalline defects (Holdren and Speyer, 1985).

The calculation of porosity has two components: total grain area (in μm^2) and pore area (in μm^2). Feldspars that had no pores (at the 0.1 μm resolution of BSE) were measured first; this cross-sectional area was given a value of 0% porosity. The BSE images of feldspars that did weather were subjected to a density slicing since they consisted of two classes: dark pores and bright plagioclase (Fig. 12). The output was a calculation of number of pixels in the unweathered section of the grain, and the number of pixels in the weathered section, where pixel areas were scaled to a cross-sectional area in square micrometers. Lastly, total cross-sectional areas (weathered and unweathered) were summed for the 100 grains from each site.[4]

Weathering Along a Single Lava Flow

Time and lithology were controlled by collecting only from the ~2885 ± 150 ^{14}C-yr-old f5d p3.5 flow (Moore and Clague,

[4]Raw data are presented in the GSA Data Repository. See footnote 1.

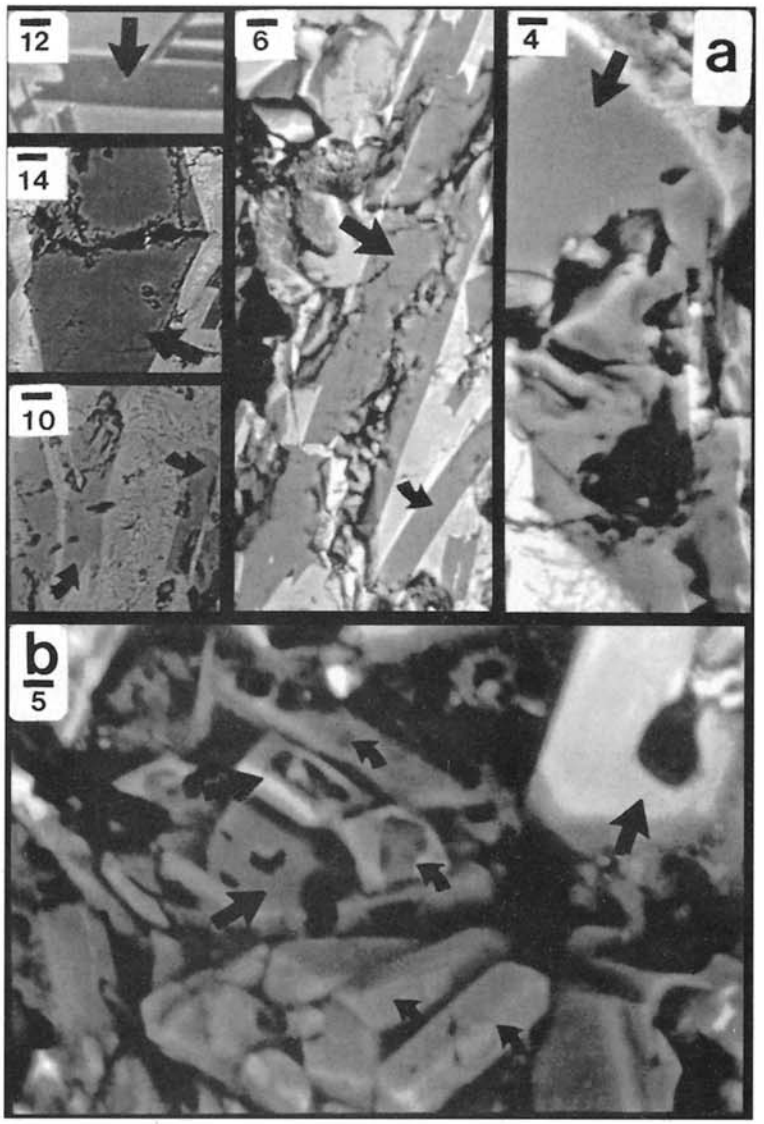

Figure 12. Plagioclase weathering on Hualalai Volcano, Hawaii. Scale bars in micrometers. (a) BSE images of polished cross section from the Puu Waawaa Ranch flow, where the typical style of plagioclase feldspar weathering by dissolution is exemplified. Smaller arrows identify plagioclase grains. The large arrow identifies the locale of a typical electron microprobe analysis of the unweathered section of the plagioclase grain: Na_2O, 3.48; MgO, 0.26; Al_2O_3, 27.84; SiO_2, 48.45; K_2O, 0.32; CaO, 16.28; TiO_2, 0.18; MnO, 0.00; FeO, 0.86. (b) BSE image of a broken weathering rind from the same site as a. Arrows identify plagioclase crystals (determined by EDS analysis).

1991). Collection sites span >1500 m from forest with ~1200 mm mean annual precipitation to near desert biomes close to sea level with <500 mm precipitation (Fig. 10). Total cross-sectional areas of plagioclase analyzed from each one of different sites ranged from 127 000 μm^2 to 156 000 μm^2.

In both organic-poor and organic-rich microenvironments, plagioclase weathering increased with elevation (more precipitation), as Johnsson et al. (1993) found in interpreting soil clay mineralogy, despite the negative factor of lower temperatures. Higher weathering rates at higher elevations are undoubtedly tied to increased moisture abundance, through reduced evapotranspiration (cooler temperatures), increased precipitation, and less insolation receipt (more clouds). The increasing offset between organic-rich and organic-poor microsites at higher elevations (Fig. 13) may be due to organic-rich microenvironments having progressively greater concentrations of organic acids and greater moisture availability trapped under the lichen cover. In contrast, organic-poor microenvironments experience more rapid water runoff, without organic acids or moisture retention by lichens.

Weathering Along an Isohyet

In the second study of plagioclase weathering, temperature varied while precipitation was held constant along the 500 mm isohyet (Giabelluca et al., 1986; Fig. 10). Samples were collected from only organic-poor sites on flows that range in age from 2000 to 2700 ^{14}C yr (Moore and Clague, 1991).[5] Since the 500 mm isohyet wraps around Hualalai in an uphill direction, mean annual temperature lowers with elevation, with values from Armstrong (1973). The same methodology as in the first study was used, but percent weathering is normalized to age, because there is some variability in age among different flows.

Figure 14 reveals that in situ weathering of plagioclase is particularly sensitive to temperature. Rates of dissolution per thousand years are not distinguishable for the two warm low elevation sites (1.07% ± 0.04% porosity/k.y. at 20 m; 0.99% ± 0.05% porosity/k.y. at 100 mm). At ~500 m, however, the rate drops to 0.78% ± 0.04%/k.y. The biggest reduction in weathering rates occurs at the 2380 m site (0.21% ± 0.04%/k.y.). The strong temperature sensitivity of plagioclase dissolution has implications for long-term climate evolution (Brady, 1991). A strong temperature dependency of plagioclase weathering is consistent with Velbel's (1993a) study of watershed chemistry and Hellmann's (1994) laboratory study. However, these results may vary with different aqueous species at surface reaction sites (Casey and Sposito, 1992). The in situ temperature dependence of plagioclase weathering, therefore, may differ under a cover of epilithic organisms.

CONCLUSION

Chemical weathering transforms the earth's crust through biogeochemical interactions with the atmosphere, biosphere, and hydrosphere. Chemical weathering is a fundamental part of a changing earth, and it is widely recognized as an important player in

[5]See footnote 1.

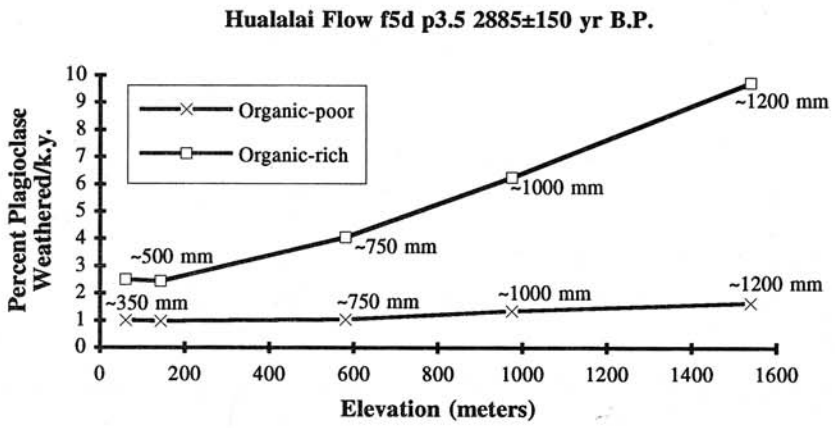

Figure 13. Plagioclase weathering trends at different elevations on flow f5d p3.5, dated at 2885 ± 150 yr B.P. (Rubin et al., 1987; Moore and Clague, 1991). Organic-rich microenvironments are directly underneath lichens. Organic-poor microenvironments are away from acid-secreting organisms and silica glazes. Approximate annual precipitation totals, interpolated from Giambelluca et al. (1986), are indicated for each elevation.

the earth's long-term evolution (Brady, 1991; Berner, 1992; Gibbs and Kump, 1994). At the interface between public policy and earth science, "estimation of the rates of mineral-water reactions at watershed, continental and global scales is of paramount importance in understanding the short- and long-term effects of natural and anthropogenic influences on the Earth system" (Brantley and Velbel, 1993, p. vii).

Great advances have been made in quantitative chemical weathering research in recent years, in the number of different approaches used to quantify weathering (Table 1), and in the adoption of more holistic perspectives that place chemical weathering within a framework of synergistic earth systems (e.g., Brimhall et al., 1991; Lasaga et al., 1994; Pope et al., 1995). Still, there is a niche not met by other techniques: measurement of mass dissolved in situ, which in turn facilitates comparisons among different units used to measure mass balances in weathering.

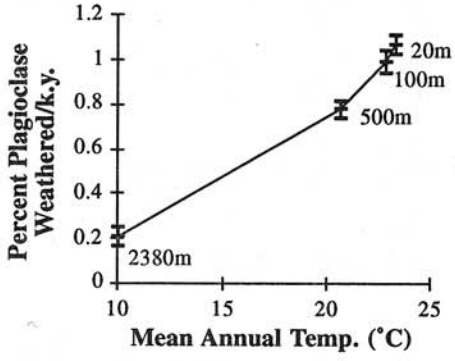

Figure 14. Plagioclase weathering trends along the 500 mm isohyet on Hualalai (based on Giambelluca, 1986), collected from flows that range in age from 2000 to 2700 ^{14}C yr (Rubin et al., 1987; Moore and Clague, 1991). Organic-poor microenvironments, away from acid-secreting organisms and away from rock coatings, are the only microsites studied. Mean annual temperatures are derived from Armstrong (1973).

The purpose of this paper is to present a microscopic method that helps fill this niche by combining two commonly used tools, digital image processing and back-scattered electron microscopy (BSE). Digital processing of BSE imagery quantifies chemical weathering from in situ dissolution. Holes appear dark in BSE, and these can be counted because they contrast greatly with adjacent mineral material that appears bright. Although there are inherent technical and field limitations to digital processing of BSE imagery, there is a wide array of weathering problems that can be addressed. Four case studies are presented that exemplify different types of weathering research: initiation of weathering forms; maintenance of weathering forms; quantifying rates of rock dissolution; and assessing the importance of temperature, precipitation, and microenvironment on plagioclase dissolution.

The first case study focuses on the relationship between in situ porosity and the initiation of small honeycomb weathering forms, subcentimeter alveoli sampled from in sandstone in central Arizona. Incipient alveoli occur where porosity exceeds ~32% in the upper 100 μm. One explanation is that, upon reaching this threshold, the resistance of sandstone to shear stresses (e.g., overland flow, lichen thalli growth) is reduced enough to allow grain detachment. Although the specific porosity value needed to develop alveoli will certainly vary with lithology, this supports the observation of Paradise (1993) that thresholds exist in the development of weathering forms.

Maintenance of weathering forms may require conditions different from inception, as in the second case study on gnamma pits and polygonal cracks in Hawaiian basalts. Coatings of silica glaze effectively freeze rock-surface erosion for a period of time, but rock weathering continues underneath the protective rock coating. Porosity gradually grows under the silica glaze until the weathering rind loses cohesion at a porosity of ~37%–47%, and both rind and silica glaze spalls. Then, the silica glaze starts to grow again, and another cycle of weathering-rind development begins.

In studies of weathering forms, pores that develop during subaerial exposure cannot be distinguished from pores inherited from past weathering in the subsurface (cf. Colin et al., 1992; Vasconcelos et al., 1992). However, the focus in the first two case studies is on the relationship between in situ porosity, weathering form, and weathering environment. In contrast, the third and fourth case studies involve measuring long-term dissolution rates in systems that do not have inherited weathering. This is possible when weathering started at an established time in the past.

The third case study concerns the measurement of rock dissolution in weathering rinds formed on wind-polished aplite boulders. Because no erosion has taken place since eolian abrasion ceased at known times in the past, weathering rates could be calculated. Using the age of the ventifacts and the density of the boulder, dissolution pores yield data on mass weathered per unit area. For the last 14 k.y., rinds 0.9 ± 0.5 mm thick lost 40 ± 15 g/m^2/k.y. Over the last 17 k.y., rinds 1.1 ± 0.6 mm lost 43 ± 16 g/m^2/k.y. Dissolution rates increased over time to 67 ± 23 g/m^2/k.y. for the last 60–65 k.y., even though weathering rinds thickened at a linear rate to 3.2 ± 1.4 mm. These values can be compared directly to units used in watershed and soil mass balance research (Table 1), unlike conventional approaches to the measurement of boulder weathering

(e.g., morphometry of weathering forms and weathering-rind thickness).

The fourth case study assesses the role of temperature, precipitation and microenvironment on rates of in situ plagioclase dissolution, where the onset of weathering is established by radiocarbon ages on 2- to 3-k.y.-old Hawaiian lava flows. Plagioclase dissolution is influenced by temperature (0.07% increase per °C), but not as much as precipitation. However, microenvironment is a more important control on weathering rate than either mean annual precipitation or temperature. Rocks close to sea level in organic-rich environments (under lichens) weather twice as fast as adjacent organic-poor environments (weathering from carbonic acid). As elevation and precipitation increase, organic-rich microsites weather even faster, until at ~1200 m they dissolve approximately seven times faster than plagioclase in adjacent organic-poor microenvironments.

In summary, digital processing of backscatter imagery offers a powerful way to study the in situ dissolution of rocks and minerals, either as a stand-alone tool or as a method that complements other approaches used in chemical weathering research.

ACKNOWLEDGMENTS

This research was supported in part by National Science Foundation Presidential Young Investigator award 8918644. This manuscript benefited from the comments of P. Beyer, G. Brimhall, F. Brown, F. Colin, D. Krinsley, G. Pope, and T. Wasklewicz. Thanks to G. Pope for permission to use his Cabo San Lucas sample, T. Liu for assistance in sample preparation, A. Bach for a modified map of his Bishop Creek ventifact sites, P. Brady for discussions on the temperature dependency of plagioclase weathering, R. Moore and F. Trusdell for introducing me to Hualalai, and J. Clark for assistance with the microprobe. The Arizona State University microprobe was purchased in part by National Science Foundation grant EAR 8408163.

REFERENCES CITED

Aborg, G., Stijfhoorn, D. E., Raheim, A., and Lofvendahl, R., 1993, Laser determination of weathering depth and provenance by carbon and oxygen isotopes, *in* Thiel, M. J., ed., Conservation of stone and other materials: London, E&FN Spon, p. 144–151.

Alpers, C., and Brimhall, G. H., 1988, Middle Miocene climatic change in the Atacama Desert, northern Chile: Evidence from supergene mineralization at La Escondida: Geological Society of America Bulletin, v. 100, p. 1640–1656.

Alpers, C., and Brimhall, G. H., 1989, Paleohydrologic evolution and geochemical dynamics of cumulative supergene metal enrichment at La Escondida, Atacama Desert, northern Chile: Economic Geology, v. 84, p. 229–255.

April, R., Newton, R., and Coles, L. T., 1986, Chemical weathering in two Adirondack watersheds: Past and present-day rates: Geological Society of America Bulletin, v. 97, p. 1232–1238.

Armstrong, R. W., 1973, Atlas of Hawaii: Honolulu, University of Hawaii Press, 222 p.

Bach, A., 1995, Eolian modifications of glacial moraines found today in a dryland environment, *in* Tchakerian, V., ed., Desert aeolian processes: New York, Chapman (in press).

Beauvais, A., and Colin, F., 1993, Evolution of iron crust systems under tropical conditions: Chemical Geology, v. 106, p. 77–101.

Benito, G., Machado, M. J., and Sancho, C., 1993, Sandstone weathering processes damaging prehistoric rock paintings at the Albarracin Cultural Park, NE Spain: Environmental Geology, v. 22, p. 71–79.

Berner, R. A., 1992, Weathering, plants, and the long-term carbon cycle: Geochimica et Cosmochimica Acta, v. 56, p. 3225–3231.

Berry, M. E., 1994, Soil-geomorphic analysis of Late-Pleistocene glacial sequences in the McGee, Pine, and Bishop Creek drainages, east-central Sierra Nevada, California: Quaternary Research, v. 41, p. 160–175.

Bird, M. I., Longstaffe, F. J., Fyfe, W. S., Kronberg, B., and Kishida, A., 1993, An oxygen-isotope study of weathering in the eastern Amazon Basin, Brazil, *in* Smart, P. K., Lohman, K. C., McKenzie, J., and Savin, S., eds., Climatic change in continental isotopic records: American Geophysical Union Geophysical Monograph 78, p. 295–307.

Birkeland, P. W., 1964, Pleistocene glaciation of the northern Sierra Nevada, north of Lake Tahoe: Journal of Geology, v. 72, p. 810–825.

Birkeland, P. W., 1984, Soils and geomorphology (second edition): New York, Oxford University Press, 372 p.

Blackwelder, E., 1931, A Pleistocene glaciation in the Sierra Nevada and Basin Ranges: Geological Society of America Bulletin., v. 42, p. 865–922.

Blum, A. F., White, A. F., Schulz, M. S., Bullen, T. D., Harden, J. W., and Peterson, M., 1994, Chemical weathering rates of minerals and soils developed on granitoid alluvium: Eos, v. 74, no. 4, p. 280.

Blum, J. D., Erel, Y., and Brown, K., 1994, $^{87}Sr/^{86}Sr$ ratios of Sierra Nevada stream waters: Implications for relative mineral weathering rates: Geochimica et Cosmochimica Acta, v. 58, p. 5019–5025.

Bluth, G.J.S., and Kump, L. R., 1994, Lithologic and climatological controls of river chemistry: Geochimica et Cosmochimica Acta, v. 58, p. 2341–2359.

Bohor, B. F., and Hughes, R. E., 1971, Scanning electron microscopy of clays and clay minerals: Clays and Clay Minerals, v. 19, p. 49–54.

Brady, P. V., 1991, The effect of silicate weathering on global temperature and atmospheric CO_2: Journal of Geophysical Research, v. 96, p. B18101–B18106.

Brantley, S. L., and Velbel, M. A., 1993, Preface to special issue on geochemical kinetics of mineral-water reactions in the field and the laboratory: Chemical Geology, v. 105, p. vii–ix.

Braun, J. J., Pagel, M., Muller, J., Bilong, P., Michard, A., Guillet, B., 1990, Cerium anomalies in lateritic profiles: Geochimica et Cosmochimica Acta, v. 54, p. 781–795.

Bricker, O. P., Godfrey, A. E., and Cleaves, E. T., 1968, Mineral-water interaction during the chemical weathering of silicates, *in* Baker, R., ed., Trace inorganics in water: Washington, D.C., American Chemical Society, p. 128–142.

Brimhall, G. H., and Dietrich, W. E., 1987, Constitutive mass balance relations between chemical composition, volume, density, porosity, and strain in metasomatic hydrochemical systems: Results on weathering and pedogenesis: Geochimica et Cosmochimica Acta, v. 51, p. 567–587.

Brimhall, G. H., Lewis, C. J., Ague, J. J., Dietrich, W. E., Hampel, H., Teague, T. and Rix, P., 1988, Metal enrichment in bauxites by deposition of chemically mature eolian dust: Nature, v. 333, p. 819–824.

Brimhall, G. H., and nine others, 1991, Deformational mass transport and invasive processes in soil evolution: Science, v. 255, p. 695–702.

Brown, E. T., Bourles, F., Colin, F., Sanfo, Z., Raisbeck, G., and Yiou, F., 1994, The development of iron crust systems in Burkina Faso, West Africa, examined with in situ produced cosmogenic nuclides: Earth and Planetary Science Letters, v. 124, p. 19–33.

Burke, R. M., and Birkeland, P. W., 1979, Re-evaluation of multiparameters relative dating techniques and their application to the glacial sequence along the eastern escarpment of the Sierra Nevada, California: Quaternary Research, v. 11, p. 21–51.

Caine, N., 1979, Rock weathering rates at the soil surface in an alpine environment: Catena, v. 6, p. 131–144.

Caine, N., 1992, Spatial patterns of geochemical denudation in a Colorado alpine environment, *in* Dixon, J. C., and Abrahams, A. D., ed., Periglacial geomorphology (Proceedings of the 22nd Annual Binghamton Geomorphology Symposium): Chichester, Wiley, p. 63–88.

Campbell, I. A., 1991, Classification of rock weathering at Writing-On-Stone Provincial Park, Alberta, Canada: Earth Surface Processes and Landforms, v. 16, p. 701–711.

Casey, W. H., and Sposito, G., 1992, On the temperature dependence of mineral dissolution rates: Geochimica Cosmochimica Acta, v. 56, p. 3825–3830.

Casey, W. H., Westrich, H. R., Banfield, J. F., Ferruzzi, G., and Arnold, G. W., 1993, Leaching and reconstruction at the surfaces of dissolving chain-silicate minerals: Nature, v. 366, p. 253–256.

Cerling, T. E., Pederson, B. L., and Von Damm, K. L., 1989, Sodium-calcium ion exchange in the weathering of shales: Implications for global weathering budgets: Geology, v. 17, p. 552–554.

Clague, D. A., Jackson, E. D., and Wright, T. L., 1980, Petrology of Hualalai Volcano, Hawaii: Implications for mantle composition: Bulletin Volcanologique, v. 43-4, p. 641–656.

Clemens, S. C., Farreell, J. W., and Gromet, L. P., 1993, Synchronous changes in seawater strontium isotope composition and global climate: Nature, v. 363, p. 607–610.

Cochran, M. F., and Berner, R., 1993, Reply *to* Comments *on* "Weathering plants and the long-term carbon cycle": Geochimica et Cosmochimica Acta, v. 57, p. 2147–2148.

Colin, F., Brimhall, G. H., Nahon, D., Baronnet, A., and Kathy, D., 1992, Equatorial rainforest lateritic mantles: A geomembrane filter: Geology, v. 20, p. 523–526.

Colin, F., Alarcon, C., and Viellard, P., 1993a, Zircon: An immobile index in soils?: Chemical Geology, v. 107, p. 273–276.

Colin, F., Viellard, P., and Ambrosi, J. P., 1993b, Behavior of gold in lateritic equatorial environments: Mass transfer and thermodynamic study: Earth and Planetary Science Letters, v. 114, p. 259–285.

Colman, S. M., 1982, Chemical weathering of basalts and andesites: Evidence from weathering rinds: U.S. Geological Survey Professional Paper 1246, p. 1–51.

Colman, S. M., and Dethier, D., editors, 1986, Rates of chemical weathering of rocks and minerals: Orlando, Florida, Academic Press.

Colman, S. M., and Pierce, K., 1981, Weathering rinds on andesitic and basaltic stones as a Quaternary age indicator, western United States: U.S. Geological Survey Professional Paper 1210, p. 1–51.

Conca, J. L., and Astor, A. M., 1987, Capillary moisture flow and the origin of cavernous weathering in dolerites of Bull Pass Antarctica: Geology, v. 15, p. 151–154.

Conca, J. L., and Rossman, G. R., 1982, Case hardening of sandstone: Geology, v. 10, p. 520–523.

Cremeens, D. L., Darmody, R. G., and Jansen, I. G., 1987, SEM analysis of weathered grains: Pretreatment effects: Geology, v. 15, p. 401–404.

Crook, R., Jr., 1986, Relative dating of Quaternary deposits based on P-wave velocities in weathered granitic clasts: Quaternary Research, v. 25, p. 281–292.

Curtiss, B., Adams, J. B., and Ghiorso, M. S., 1985, Origin, development and chemistry of silica-alumina rock coatings from the semiarid regions of the island of Hawaii: Geochimica et Cosmochimica Acta, v. 49, p. 49–56.

Danin, A., 1985, Palaeoclimates in Israel: Evidence from weathering patterns of stones in and near archaeological sites: Bulletin of the American Schools of Oriental Research, v. 259, p. 33–43.

Day, M. J., and Goudie, A. S., 1977, Field assessment of rock hardness using the Schmidt Test Hammer: British Geomorphological Research Group Technical Bulletin, v. 18, p. 19–29.

Dearman, W. R., Baynes, F. J., and Irfan, T. Y., 1978, Engineering grading of weathered granite: Engineering Geology, v. 12, p. 345–374.

Dethier, D. P., 1988, A hydrogeochemical model for stream chemistry, Cascade Range, Washington, U.S.A.: Earth Surface Processes and Landforms, v. 13, p. 321–333.

Dilks, A., and Graham, S. C., 1985, Quantitative mineralogical characterization of sandstones by back-scattered electron image analysis: Journal of Sedimentary Petrology, v. 55, p. 347–355.

Dixon, J. C., Thorn, C. E., and Darmody, R. G., 1984, Chemical weathering processes on the Vantage Peak nunatak, Juneau Icefield, southern Alaska: Physical Geography, v. 5, p. 111–131.

Dorn, R. I., and eight others, 1992, Rock varnish on Hualalai and Mauna Kea Volcanoes, Hawaii: Pacific Science, v. 46, p. 11–34.

Dragovich, D., 1969, The origin of cavernous surfaces (tafoni) in granitic rocks of southern Australia: Zeitschrift für Geomorphology, v. 13, p. 163–181.

Dragovich, D., 1986, Weathering rates of marble in urban environments, eastern Australia: Zeitschrift für Geomorphologie, v. 30, p. 203–214.

Drever, J. I., and Zobrist, J., 1992, Chemical weathering of silicate rocks as a function of elevation in the southern Swiss Alps: Geochimica et Cosmochimica Acta, v. 56, p. 3209–3216.

Dryden, L., and Drydan, C., 1946, Comparative rates of weathering of some common heavy minerals: Journal of Sedimentary Petrology, v. 16, p. 91–96.

Eggleton, R. A., 1986, The relation between crystal structure and silicate weathering rates, *in* Colman, S. M., and Dethier, D. P., ed., Rates of chemical weathering of rocks and minerals: Orlando, Florida, Academic Press, p. 21–40.

Ehrlich, R., Kennedy, S. K., Crabtree, S. J., and Cannon, R. L., 1984, Petrographic image analysis, I. Analysis of reservoir complexes: Journal of Sedimentary Petrology, v. 54, p. 1365–1378.

Ehrlich, R., Crabtree, S. J., Horkowitz, K. O., and Horkowitz, J. P., 1991, Petrography and reservoir physics, I: Objective classification of reservoir porosity: American Association of Petroleum Geologists Bulletin, v. 75, p. 1547–1562.

Emery, K. O., 1960, Weathering of the Great Pyramid: Journal of Sedimentary Petrology, v. 30, p. 140–143.

Erel, Y., Harlaron, Y., and Blum, J. D., 1994, Lead isotope systematics of granitoid weathering: Geochimica et Cosmochimica Acta, v. 58, p. 5299–5306.
Fahey, B. D., 1986, Weathering pit development in the central Otago Mountains of southern New Zealand: Arctic and Alpine Research, v. 18, p. 337–348.
Farr, T., and Adams, J. B., 1984, Rock coatings in Hawaii: Geological Society of America Bulletin, v. 95, p. 1077–1083.
Fuller, C. M., and Sharp, J. M., 1992, Permeability and fracture patterns in extrusive volcanic rocks: Implications from welded Santana Tuff, Trans-Pecos, Texas: Geological Society of America Bulletin, v. 104, p. 1485–1496.
Giambelluca, T. W., Mullet, M. A., and Schroder, T. A., 1986, Rainfall atlas of Hawaii: Honolulu, Hawaii, Department of Land and Natural Resources.
Gibbs, M. T., and Kump, L. R., 1994, Global chemical erosion during the last glacial maximum and the present: Sensitivity to changes in lithology and hydrology: Paleoceanography, v. 9, p. 529–543.
Gibson, E. K., Bustin, R., and Wentworth, S., 1982, Development of regoliths in Mars-like environments: Lunar and Planetary Science, v. 13, p. 259–260.
Giles, M. R., and Marshall, J. D., 1986, Constraints on the development of secondary porosity in the subsurface: Re-evaluation of processes: Marine and Petroleum Geology, v. 3, p. 243–255.
Gosse, J. C., Grant, D. R., Klein, J., Klassen, R. A., Evenson, E. B., Lawn, B., and Middleton, R., 1993, Significance of altitudinal weathering zones in Atlantic Canada, inferred from in situ produced cosmogenic radionuclides: Geological Society of America Abstracts with Programs, v. 25, no. 6, p. A394.
Goudie, A. S., Anderson, M., Burt, T., Lewin, J., Richards, K., Whalley, B., and Worsley, P., editors, 1990, Geomorphological techniques (second edition): London, Unwin Hyman, 570 p.
Grant, W. H., 1969, Abrasion pH, an index of weathering: Clays and Clay Minerals, v. 17, p. 151–155.
Hall, R. D., and Horn, L. L., 1993, Rates of hornblende etching in soils in glacial deposits of the northern Rocky Mountains (Wyoming-Montana, U.S.A.): Influence of climate and characteristics of the parent material: Chemical Geology, v. 105, p. 17–29.
Hellmann, R., 1994, The albite-water system: Part I. The kinetics of dissolution as a function of pH at 100, 200, and 300 °C: Geochimica et Cosmochimica Acta, v. 58, p. 595–611.
Hobbs, W. H., 1917, The erosional and degradational processes of deserts, with especial reference to the origin of desert depressions: Annals of the Association of American Geographers, v. 7, p. 25–60.
Holdren, G.R.J., and Speyer, P. M., 1985, Reaction rate-surface area relationships during the early stages of weathering—I. Initial observations: Geochimica et Cosmochimica Acta, v. 49, p. 675–681.
Ilier, I. G., 1956, An attempt to estimate the degree of weathering of intrusive rocks from their physico-mechanical properties: Proceedings, 1st International Congress of the Society of Rock Mechanics, v. 2, p. 109.
Jenny, H., 1941, Factors of soil formation: New York, McGraw Hill, 281 p.
Jensen, J. R., 1986, Introductory digital image processing: Englewood Cliffs, New Jersey, Prentice-Hall, 379 p.
Johnsson, M. J., Ellen, S. D., and McKittrick, M. A., 1993, Intensity and duration of chemical weathering: An example from soil clays of southeastern Koolau Mountains, Oahu, Hawaii: Geological Society of America Special Paper 284, p. 147–170.
Kiernan, K. W., 1980, Pleistocene glaciation of the central West Coast Range, Tasmania [B.A. thesis]: Hobart, Australia, Department of Geography, University of Tasmania.
Kiernan, K. W., 1990, Weathering as an indicator of the age of Quaternary glacial deposits in Tasmania: Australian Geographer, v. 21, p. 1–17.
Krauskopf, K. B., 1967, Introduction to geochemistry: New York, McGraw Hill, 721 p.
Krinsley, D., and Manley, C., 1989, Backscattered electron microscopy as an advanced technique in petrography: Journal of Geological Education, v. 37, p. 202–209.
Krinsley, D., Nagy, B., Dypvik, H., and Rigali, M., 1993, Microtextures in mudrocks as revealed by backscattered electron imaging: Precambrian Research, v. 61, p. 191–207.
Kurz, M. D., Colodner, D., Trull, T. W., Moore, R. B., and O'Brien, K., 1990, Cosmic ray exposure age dating in situ produced cosmogenic He-3: Results from young Hawaiian lava flows: Earth and Planetary Science Letters, v. 97, p. 177–189.
Lasaga, A. C., and Blum, A. E., 1986, Surface chemistry, etch pits, and mineral-water reactions: Geochimica et Cosmochimica Acta, v. 50, p. 2363–2379.
Lasaga, A. C., Soler, J., Ganor, J., Burch, T., and Nagy, K. L., 1994, Chemical weathering rate laws and global geochemical cycles: Geochimica et Cosmochimica Acta, v. 58, p. 2361–2381.
Likens, G. E., Bormann, F. H., Pierce, R. S., Easton, J. S., and Johnson, N. M., 1977, Biogeochemistry of a forested ecosystem: New York, Springer-Verlag.
Lowe, D. J., 1986, Controls on the rates of weathering and clay mineral genesis in airfall tephras: A review and New Zealand case study, *in* Colman, S. M., and Dethier, D., eds., Rates of chemical weathering of rocks and minerals: Orlando, Florida, Academic Press, p. 265–330.
Lundqvist, J., 1988, The Revsund area, central Jamtland—An example of preglacial weathering and landscape formation: Geografiska Annaler, v. 70A, p. 291–298.
Lyman, R. L., and Fox, G. L., 1989, A critical evaluation of bone weathering as an indication of bone assemblage formation: Journal of Archaeological Science, v. 16, p. 293–317.
MacInnis, I. N., and Brantley, S. L., 1993, Development of etch pit size distributions on dissolving minerals: Chemical Geology, v. 105, p. 31–49.
Mahaney, W., 1990, Ice on the equator; Quaternary geology of Mount Kenya, East Africa: Sister Bay, Wisconsin, Wm Caxton, 394 p.
Matsukura, Y., and Matsuoka, N., 1991, Rates of tafoni weathering on uplifted shore platforms in Nojima-Zaki, Boso Peninsula, Japan: Earth Surface Processes and Landforms, v. 16, p. 51–56.
McCarroll, D., and Nesje, A., 1993, The vertical extent of ice sheets in Nordfjord, western Norway: Measuring degree of rock surface weathering: Boreas, v. 22, p. 255–265.
McGreevy, J. P., and Smith, B. J., 1984, The possible role of clay minerals in salt weathering: Catena, v. 11, p. 169–175.
McLennan, S. M., 1993, Weathering and global denudation: Journal of Geology, v. 101, p. 295–303.
Meierding, T. C., 1993a, Marble tombstone weathering and air pollution in North America: Annals of the Association of American Geographers, v. 83, p. 568–588.
Meierding, T. C., 1993b, Inscription legibility method for estimating rock weathering rates: Geomorphology, v. 6, p. 273–286.
Melton, M. A., 1965, Debris-covered hillslopes of the southern Arizona desert: Consideration of their stability and sediment contribution: Journal of Geology, v. 73, p. 715–729.
Merino, E., Nahon, D., and Wang, Y., 1993, Kinetics and mass transfer of pseudomorphic replacement: Applications to replacement of parent minerals and kaolinite by Al, Fe, and Mn oxides during weathering: American Journal of Science, v. 293, p. 135–155.
Merritts, D. J., Chadwick, O. A., Hendricks, D. M., Brimhall, G. H., and Lewis, C. J., 1992, The mass balance of soil evolution on late Quaternary marine terraces, northern California: Geological Society of American Bulletin, v. 104, p. 1456–1470.
Milnes, A. R., and Fitzpatrick, R. W., 1989, Titanium and zirconium minerals, *in* Minerals in soil environments (second edition): Madison, Wisconsin, Soil Science Society of America Book Series, No. 1, p. 1131–1205.
Monaghan, M. C., McKean, J., Dietrich, W., and Klein, J., 1992, ^{10}Be chronometry of bedrock-to-soil conversion rates: Earth and Planetary Science Letters, v. 111, p. 483–492.
Moore, R. B., and Clague, D. A., 1991, Geologic map of Hualalai Volcano, Hawaii: U.S. Geological Survey Miscellaneous Investigation Series Map, v. I-2133, scale 1:50 000.
Moore, R. B., Clague, D. A., Rubin, M., and Borhson, W., 1987, Hualalai volcano: A preliminary summary of geologic, petrologic and geophysical data: U.S. Geological Survey Professional Paper 1350, p. 571–585.
Moran, C., Bratney, A., and Koppi, A., 1988, A micromorphometric method for estimating changing in volume of soil induced by weathering: Journal of Soil Science, v. 39, p. 357–373.
Mottershead, D. N., and Pye, K., 1994, Tafoni on coastal slopes, South Devon, U.K.: Earth Surface Processes and Landforms, v. 19, p. 543–563.
Mustoe, G. E., 1982, The origin of honeycombed weathering: Geological Society of America Bulletin, v. 93, p. 108–115.
Nahon, D., 1991, Introduction to the petrology of soils and chemical weathering: New York, Wiley and Sons.
Nesbitt, H. W., and Wilson, R. E., 1992, Recent chemical weathering of basalts: American Journal of Science, v. 292, p. 740–777.
Ogelman, Y. G., and Kapur, S., 1982, Thermoluminescence reveals weathering stages in basaltic rocks: Nature, v. 296, p. 231–232.
Paradise, T. R., 1993, Analysis of weathering-constrained erosion of sandstone in the Roman Theater of Petra, Jordan, [Ph.D. dissert.]: Tempe, Department of Geography, Arizona State University, 202 p.
Pavich, M. J., 1986, Processes and rates of saprolite production and erosion on a foliated granitic rock of the Virginia Piedmont, *in* Colman, S. M., and Dethier, D., eds., Rates of chemical weathering of rocks and minerals: Orlando, Florida, Academic Press, p. 551–590.
Pentecost, A., 1991, The weathering rates of some sandstone cliffs, central Weald, England: Earth Surface Processes and Landforms, v. 16, p. 83–91.
Pope, G. A., 1995, Newly discovered submicron-scale weathering in quartz: Geographical implications: Professional Geographer, v. 47 (in press).
Pope, G. A., Dorn, R. I., and Dixon, J., 1995, A new conceptual model for understanding geographical variations in weathering: Annals of the Association of American Geographers, v. 85, p. 38–64.
Probst, J. L., Mortatti, J., and Tardy, Y., 1994, Carbon river fluxes and weathering CO_2 consumption in the Congo and Amazon river basins: Applied Geochemistry, v. 9, p. 1–13.
Pye, K., and Krinsley, D., 1984, Petrographic examination of sedimentary rocks in the SEM using backscattered detectors: Journal of Sedimentary Petrology, v. 54, p. 877–888.
Reiche, P., 1945, A survey of weathering processes and products: University of New Mexico Publications in Geology 1, p. 1–87.
Robert, M., and Tessier, D., 1992, Incipient weathering: Some new concepts on weathering, clay formation and organization, *in* Martini, I. P., and Chesworth, W., eds., Weathering, soils and Paleosols: Amsterdam, Netherlands, Elsevier, p. 71–105.
Rubin, M., Gargulinksi, L. K., and McGeehin, J. P., 1987, Hawaiian radiocarbon dates: U.S. Geological Survey Professional Paper 1350, p. 213–242.
Schirrmeister, L., and Störr, M., 1994, The weathering of basaltic rocks in Burundi and Vietnam: Catena, v. 21, p. 243–256.
Schott, J., and Petit, J.-C., 1987, New evidence for the mechanisms of dissolution of silicate minerals, *in* Stumm, W., ed., Aquatic surface chemistry: New York, Wiley and Sons, p. 293–315.
Schwartzman, D. W., and Volk, T., 1991, Biotic enhancement of weathering and surface temperatures on earth since the origin of life: Palaeogeography, Palaeoclimatology, Palaeoecology, v. 90, p. 357–371.
Sharp, R. P., 1969, Semiquantitative differentiation of glacial moraines near Convict Lake, Sierra Nevada, California: Journal of Geology, v. 77, p. 68–91.
Shur, A. S., Anufriyev, Y. N., and Yel-kina, N. T., 1966, Ultra- and microporosity of quartz crystals [in Russian]: Vsesoyuznogo Mineralojicheskogo Obshchestovo Zapiski, v. 95, no. 6, p. 743–748.
Souchez, R., Lemmens, M., Lorrain, R., Tison, J., Jouzel, J., and Sugden, D., 1990, Influence of hydroxyl-bearing minerals on the isotopic composition of ice from the basal zone of an ice sheet: Nature, v. 345, p. 244–246.
Steward, A. D., 1993, The ratio of mechanical to chemical denudation in alluvial systems, derived from geochemical mass balance: Transactions of the Royal Society of Edinburgh: Earth Sciences, v. 84, p. 73–78.
Sverdrup, H., and Warfvinge, P., 1993, Calculating field weathering rates using a mechanistic geochemical model PROFILE: Applied Geochemistry, v. 8, p. 273–283.
Swoboda-Colberg, N. G., and Drever, J. I., 1993, Mineral dissolution rates in plot-scale field and laboratory experiments: Chemical Geology, v. 105, p. 51–69.
Tchakerian, V. P., 1991, Late Quaternary aeolian geomorphology of Dale Lake sand sheet, southern Mojave Desert, California: Physical Geography, v. 12, p. 347–369.
Trudgill, S. T., Crabtree, R. B., Ferguson, R. I., Ball, J., and Gent, R., 1994, Ten year remeasurement of chemical denudation on a magnesian limestone hillslope: Earth Surface Processes and Landforms, v. 19, p. 109–114.
Twidale, C. R., 1982, Granite landforms: Amsterdam, Netherlands, Elsevier.
Vasconcelos, P. M., Becker, T. A., Renne, P. R., and Brimhall, G. H., 1992, Age and duration of weathering by K-Ar and Ar-Ar analysis of potassium-manganese oxides: Science, v. 258, p. 451–455.
Velbel, M. A., 1986, The mathematical basis for determining rates of geochemical and geomorphic processes in small forested watersheds by mass balance: Examples and implications, *in* Colman, S. M., and Dethier, D. P., ed., Rates of chemical weathering of rocks and minerals: Orlando, Florida, Academic Press, p. 439–451.
Velbel, M. A., 1993a, Temperature dependence on silicate weathering in nature: How strong a negative feedback on long-term accumulation of atmospheric CO_2 and global greenhouse warming?: Geology, v. 21, p. 1059–1062.
Velbel, M. A., 1993b, Constancy of silicate-mineral weathering-rate ratios between natural and experimental weathering: Implications for hydrologic control of differences in absolute rates: Chemical Geology, v. 105, p. 89–99.
Viles, H. A., and Trudgill, S. T., 1984, Long term remeasurement of micro-erosion meter rates, Aldabra Atoll, Indian Ocean: Earth Surface Processes and Landforms, v. 9, p. 89–94.
Wakatsuki, T., and Rasyidin, A., 1992, Rates of weathering and soil formation: Geoderma, v. 52, p. 251–263.
Wasklewicz, T., 1994, Importance of environment on the order of mineral weathering in olivine basalts, Hawaii: Earth Surface Processes and Landforms, v. 19, p. 715–735.
Watts, S. H., 1985, A scanning electron microscope study of bedrock microfractures in granites under high arctic conditions: Earth Surface Processes and Landforms, v. 10, p. 161–172.
Welch, S. A., and Ullman, W. J., 1993, The effect of organic acids on plagioclase dissolution rates and stoichiometry: Geochimica et Cosmochimica Acta, v. 57, p. 2725–2736.
Whalley, W. B., Douglas, G. R., and McGreevy, J. P., 1982, Crack propagation and associated weathering in igneous rocks: Zeitschrift für Geomorphology, v. 26, p. 33–54.
White, A. F., and Hochella, M. F., 1992, Surface chemistry associated with the cooling and subaerial weathering of recent basalt flows: Geochimica et Cosmochimica Acta, v. 56, p. 3711–3721.
Williams, R., and Robinson, D., 1989, Origin and distribution of polygonal cracking of rock surfaces: Geografiska Annaler, v. 71A, p. 145–159.
Yapp, C. J., and Poths, H., 1992, Ancient atmospheric CO_2 pressures inferred from natural goethites: Nature, v. 355, p. 342–344.
Yatsu, E., 1988, The nature of weathering: An introduction: Tokyo, Sozosha, 624 p.
Young, R., and Young, A., 1992, Sandstone landforms: Berlin, Springer-Verlag, 163 p.

MANUSCRIPT RECEIVED BY THE SOCIETY JANUARY 27, 1994
REVISED MANUSCRIPT RECEIVED NOVEMBER 26, 1994
MANUSCRIPT ACCEPTED NOVEMBER 29, 1994

Printed in U.S.A.